JACS
JOURNAL OF THE AMERICAN CHEMICAL SOCIETY

ARTICLE

pubs.acs.org/JACS

Systematic Investigation of the Metal-Structure−Photophysics Relationship of Emissive d^{10}-Complexes of Group 11 Elements: The Prospect of Application in Organic Light Emitting Devices

Chien-Wei Hsu,[†] Chao-Chen Lin,[‡] Min-Wen Chung,[‡] Yun Chi,*[,†] Gene-Hsiang Lee,[‡] Pi-Tai Chou,*[,‡] Chih-Hao Chang,*[,§] and Pin-Yang Chen[§]

[†]Department of Chemistry, National Tsing Hua University, Hsinchu 30013, Taiwan

[‡]Department of Chemistry, National Taiwan University, Taipei 10617, Taiwan

[§]Department of Photonics Engineering, Yuan Ze University, Chungli 32003, Taiwan

Supporting Information

ABSTRACT: A series of new emissive group 11 transition metal d^{10}-complexes **1**−**8** bearing functionalized 2-pyridyl pyrrolide together with phosphine ancillary such as bis[2-(diphenylphosphino)phenyl] ether (POP) or PPh_3 are reported. The titled complexes are categorized into three classes, i.e. Cu(I) complexes (**1**−**3**), Ag(I) complexes (**4** and **5**), and Au(I) metal complexes (**6**−**8**). Via combination of experimental and theoretical approaches, the group 11 d^{10}-metal ions versus their structural variation, stability, and corresponding photophysical properties have been investigated in a systematic and comprehensive manner. The results conclude that, along the same family, how much a metal d-orbital is involved in the electronic transition plays a more important role than how heavy the metal atom is, i.e. the atomic number, in enhancing the spin−orbit coupling. The metal ions with and without involvement of a d orbital in the lowest lying electronic transition are thus classified into internal and external heavy atoms, respectively. Cu(I) complexes **1**−**3** show an appreciable metal d contribution (i.e., MLCT) in the lowest lying transition, so that Cu(I) acts as an internal heavy atom. Despite its smallest atomic number among group 11 elements, Cu(I) complexes **1**−**3** exhibit a substantially larger rate of intersystem crossing (ISC) and phosphorescence radiative decay rate constant (k_r^P) than those of Ag(I) (**4** and **5**) and Au(I) (**6**−**8**) complexes possessing pure $\pi \rightarrow \pi^*$ character in the lowest transition. Since Ag(I) and Au(I) act only as external heavy atoms in the titled complexes, the spin−orbit coupling is mainly governed by the atomic number, such that complexes associated with the heavier Au(I) (**6**−**8**) show faster ISC and larger k_r^P than the Ag(I) complexes (**4** and **5**). This trend of correlation should be universal and has been firmly supported by experimental data in combination with empirical derivation. Along this line, Cu(I) complex **1** exhibits intensive phosphorescence (Φ_p = 0.35 in solid state) and has been successfully utilized for fabrication of OLEDs, attaining peak EL efficiencies of 6.6%, 20.0 cd/A, and 14.9 lm/W for the forward directions.

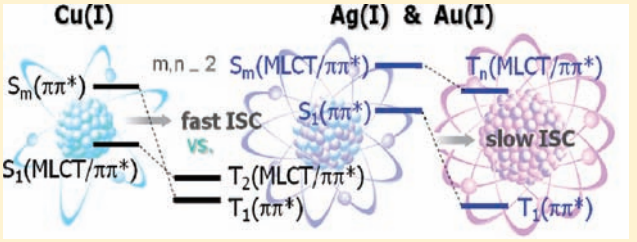

1. INTRODUCTION

There has been considerable interest in the fundamental properties of luminescent transition metal complexes, for which the characteristics of the lowest lying triplet excited states are dominated by both ligand-centered $\pi\pi^*$ and metal-to-ligand charge transfer (MLCT) transitions.[1] In moving toward realization of all phosphorescent organic-light emitting devices (PhOLEDs), efforts have been made to design metal-based phosphors with emission wavelengths spanning the whole visible region.[2] These research works are mainly focused on the late transition metal containing materials, for which the most recognizable paradigms involve the third-row transition metal complexes with either d^6- or d^8-electronic configuration. Guided by this initiative, our group has initiated research on Os(II), Ir(III), and Pt(II) metal complexes with pyridyl azolate and respective functionalized chelates, which are known to constitute an integral component for harnessing effective radiative transitions.[3] It is believed that the rigid metal−chelate bonding, higher ligand field strength, and the lower oxidation states of the central metal ion all play pivotal roles in facilitating the heavy-metal induced spin−orbit interaction as well as in the promotion of MLCT contributions in the emissive states.[4]

The above interest then stimulates parallel studies aimed at the investigation of emissive metal complexes that possess the d^{10}-electronic configuration.[5] However, in contrast to the luminescent Cu(I) cluster complexes,[6] the majority of monometallic Cu(I) complexes are cationic in nature, and their assembly requires the incorporation of two diimine chelates for full occupation of the tetrahedral coordination environment.[7] Recently, attention was paid to the alternative architecture possessing one diimine plus an ancillary bis-phosphine chelate,[8] due to the greatly enhanced emission performance imposed by the highly rigid and stronger

Received: March 24, 2011
Published: June 28, 2011

 © 2011 American Chemical Society

metal-phosphine bonding. With respect to the photophysics, their room temperature photoluminescence is attributed to the MLCT transition, which is enhanced by both the low oxidation potential of the Cu(I) core and the absence of a higher lying metal centered dd-transition, the latter of which would result in the weakening of metal−ligand bonding and in turn promote the radiationless deactivation in d^6- and d^8-metal complexes. In other words, for these Cu(I) complexes, the highest occupied molecular orbital (HOMO) has a predominant metal d character, possibly mixed with a small contribution from the bis-phosphine, while the lowest unoccupied molecular orbital (LUMO) is essentially residing on the π^* orbital localized on the diimine. In the absence of the aforementioned metal dd state induced quenching, they are thus capable of generating efficient luminescence and are prospective in the fabrication of OLEDs[9] as well as the light-emitting electrochemical cell (LEC)[10] with relatively low cost compared to the case of those constituted of Os(II), Ir(III), and Pt(II) complexes. Another important issue of applicability lies in that the Cu(I) complexes, in comparison to the late transition metal complexes, are more environmentally benign. Also, it is worthy of note that mobile ionic species are used in the electroluminescent layers of LEC to yield efficient light output; thus, the employment of cationic Cu(I) complexes is especially suitable.

Herein, we report the synthesis and characterization of a new class of Cu(I) metal complexes with a series of tailor-made pyrrolide anions, demonstrating various degrees of π-conjugation and spatial bulkiness. All of these compounds are luminescent, and they are unique in their high quantum efficiency (Φ > 0.3 for complex **1**) and tunable emission peak wavelengths (550−605 nm) in CH_2Cl_2 solution at room temperature, for which their luminescent behaviors are comparable to those of the three-coordinate Cu(I) complexes recently documented in the literature.[11] Experiments were then conducted to demonstrate their usefulness in fabrication of OLEDs. Moreover, for further analysis of the effects exerted by the central Cu(I) metal, we have also synthesized the Ag(I) as well as Au(I) counterparts of the group 11 triads, cf. complexes **4**−**8**, and then systematically investigated their structural versus corresponding spectroscopic and photophysical properties. In theory, the second and third row analogues of group 11 d^{10}-metal elements, on the one hand, would reveal a steady increase of atomic number, molecular mass, and ligand−metal coordination bond strength. On the other hand, they may concomitantly display a decrease of coordination numbers and an increase of oxidation potential that play adverse effects toward achieving effective luminescence. On this basis, we then provide an in-depth analysis to elucidate a puzzling exception regarding why the Cu(I) complexes are deviated from the "heavy-atom effect", a theory which states that increased intersystem crossing (ISC) rates typically accompany complexes with atoms of higher atomic number (Z). With the possession of whole group 11 metal complexes, the interplay of countering effects on the luminescent characteristics can thus be judiciously identified via the relevant photophysical studies. Such an investigation is complementary to the recent study on the relativistic effects in homogeneous Au(I) catalysis versus that of its lighter congeners.[12]

2. EXPERIMENTAL SECTION

General Information and Materials. Mass spectra were obtained on a JEOL SX-102A instrument operating in electron impact (EI) mode or fast atom bombardment (FAB) mode. ^{1}H and ^{13}C NMR spectra were recorded on Varian Mercury-400 or INOVA-500 instruments; chemical shifts are quoted with respect to the internal standard tetramethylsilane for ^{1}H and ^{13}C NMR data. Elemental analyses were carried out at the NSC Regional Instrumentation Center at National Chao Tung University, Hsinchu, Taiwan. The chelating pyrroles, namely, 3,5-bis(trifluoromethyl)-2-(2′-pyridyl) pyrrole (fpyroH), 3,5-bis(trifluoromethyl)-2- (6′-phenyl-2′-pyridyl) pyrrole (fphroH), and 3,5-bis(trifluoromethyl)-2-(2′-isoquinolinyl) pyrrole (fiqroH), were prepared according to the literature procedures,[13] while the copper complex $[Cu(CH_3CN)_4]BF_4$ was synthesized by dropwise addition of aqueous HBF_4 (50%) into a suspension of Cu_2O in acetonitrile.[14] All reactions were conducted under N_2 atmosphere using anhydrous solvents or solvents treated with an appropriate drying reagent.

Preparation of Cu(POP)(fpyro) (1). A 25 mL round bottle flask was charged with $[Cu(CH_3CN)_4]BF_4$ (50 mg, 0.16 mmol) in 10 mL of acetonitrile and bis[2-(diphenylphosphino)phenyl] ether (POP, 85.6 mg, 0.16 mmol) in 10 mL of THF. After stirring at RT for 1 h, a solution of 3,5-bis(trifluoromethyl)-2-(2′-pyridyl) pyrrole (fpyroH, 45 mg, 0.16 mmol) in 10 mL of THF was added. This mixture was stirred for another 5 h and solvent was then evaporated. Light green crystals were obtained by diffusion of hexanes into a CH_2Cl_2 solution of product at RT. Yield: 87 mg, 62%.

Spectral data for **1**: MS (FAB, ^{63}Cu): m/z 881 [M$^+$]. ^{1}H NMR (400 MHz, d_6-acetone, 298 K): δ 7.87−7.84 (m, 2H), 7.68 (t, J = 7.2 Hz, 1H), 7.40−7.38 (m, 3H), 7.30−7.22 (m, 10H), 7.16−7.08 (m, 7H), 6.98 (t, J = 7.6 Hz, 3H), 6.86−6.74 (m, 3H), 6.68−6.67 (m, 3H), 6.60 (t, J = 6.4 Hz, 1H). ^{31}P−{^{1}H} NMR (202 MHz, d_6-acetone, 298 K): δ −12.57 (br, 2P). ^{19}F−{^{1}H} NMR (470 MHz, d_6-acetone, 298 K): δ −54.19 (s, 3F), −59.22 (s, 3F). Anal. Calcd for $C_{47}H_{33}CuF_6N_2OP_2$: C, 64.06; H, 3.77; N, 3.18. Found: C, 64.08; H, 3.89; N, 3.18.

Selected crystal data of **1**: $C_{51}H_{41}CuF_6N_2O_2P_2$, M = 953.34, monoclinic, space group $C2/c$, T = 150(2) K, a = 37.5399(17), b = 12.9489(6), c = 22.7366(10) Å, β = 127.247(1)°, V = 8798.0(7) Å^3, Z = 8, ρ_{calcd} = 1.439 mg/m^3, F(000) = 3920, λ(Mo Kα) = 0.7107 Å, μ = 0.639 mm^{-1}, crystal size = 0.50 × 0.40 × 0.15 mm^3, 10105 independent reflections collected with (R_{int} = 0.0324), GOF = 1.107, final $R_1[I > 2\sigma(I)]$ = 0.0584, wR_2(all data) = 0.1742, and D-map, max./min. = 1.644/−1.121 e/Å^3.

Preparation of Cu(POP)(fphro) (2). Similar procedures are employed for the reaction of $[Cu(CH_3CN)_4]BF_4$ with POP and fphroH, giving light green crystals with a yield of 67%.

Spectral data for **2**: MS (FAB, ^{63}Cu): m/z 957 [M$^+$]. ^{1}H NMR (400 MHz, d_6-acetone, 298 K): δ 7.68 (d, J = 8.0 Hz, 1H), 7.59 (t, J = 7.6 Hz, 1H), 7.56 (d, J = 7.2 Hz, 1H), 7.40−7.20 (m, 20H), 6.92−6.84 (m, 5H), 6.80−6.72 (m, 5H), 6.60−6.58 (m, 4H). ^{31}P−{^{1}H} NMR (202 MHz, d_6-acetone, 298 K): δ −16.03 (br, 2P). ^{19}F−{^{1}H} NMR (470 MHz, d_6-acetone, 298 K): δ −53.57 (s, 3F), −60.74 (s, 3F). Anal. Calcd for $C_{53}H_{37}CuF_6N_2OP_2$: C, 66.49; H, 3.90; N, 2.93. Found: C, 66.33; H, 4.25; N, 3.27.

Selected crystal data of **2**: $C_{55}H_{41}Cl_4CuF_6N_2OP_2$, M = 1127.18, monoclinic, space group $P2_1/n$, T = 150(2) K, a = 13.9226(9), b = 20.2681(12), c = 18.1130(10) Å, β = 90.146(1)°, V = 5111.2(5) Å^3, Z = 4, ρ_{calcd} = 1.465 mg/m^3, F(000) = 2296, λ(Mo Kα) = 0.7107 Å, μ = 0.763 mm^{-1}, crystal size = 0.42 × 0.40 × 0.35 mm^3, 11736 independent reflections collected with (R_{int} = 0.0303), GOF = 1.029, final $R_1[I > 2\sigma(I)]$ = 0.0443, wR_2(all data) = 0.1092, and D-map, max./min. = 1.285/−0.910 e/Å^3.

Preparation of Cu(POP)(fiqro) (3). Similar procedures are employed for the reaction of $[Cu(CH_3CN)_4]BF_4$ with POP and fiqroH, giving yellow crystals with yield of 76%.

Spectral data for **3**: MS (FAB, ^{63}Cu): m/z 931 [M$^+$]. ^{1}H NMR (500 MHz, d_6-acetone, 298 K): δ 8.31 (d, J = 9.5 Hz, 1H), 7.96 (d, J = 9.0 Hz, 1H), 7.85 (d, J = 8.5 Hz, 1H), 7.72 (d, J = 7.5 Hz, 1H), 7.50−7.36 (m, 4H), 7.36−7.26 (m, 4H), 7.24−7.08 (m, 8H), 7.08−6.96 (m, 6H),

6.92−6.80 (m, 5H), 6.79−6.69 (m, 3H), 6.63 (t, J = 7.7 Hz, 1H). $^{31}P-\{^1H\}$ NMR (202 MHz, d_6-acetone, 298 K): δ −12.24 (br, 2P). $^{19}F-\{^1H\}$ NMR (470 MHz, d_6-acetone, 298 K): δ −53.62 (s, 3F), −58.81 (s, 3F). Anal. Calcd for $C_{51}H_{35}CuF_6N_2OP_2$: C, 65.77; H, 3.79; N, 3.01. Found: C, 65.88; H, 3.98; N, 3.37.

Preparation of Ag(POP)(fpyro) (4). A 50 mL round bottle flask was charged with Ag_2O (22.5 mg, 0.10 mmol), POP (104.8 mg, 0.20 mmol), and fpyroH (54.5 mg, 0.20 mmol) in 30 mL of CH_2Cl_2. After the mixture was stirred for 6 h at RT, the solvent was evaporated. A colorless crystalline sample was obtained by diffusion of hexanes into a CH_2Cl_2 solution at RT. Yield: 150.8 mg, 81%.

Spectral data for **4**: MS (FAB, ^{107}Ag): m/z 1032 [M^+ + ^{107}Ag], 646 [M^+ − fpyro]. ^1H NMR (500 MHz, d_6-acetone, 298 K): δ 7.89 (d, J = 4.5 Hz, 1H), 7.82 (d, J = 7.5 Hz, 1H), 7.71 (t, J = 7.5 Hz, 1H), 7.36 (t, J = 7.0 Hz, 4H), 7.32−7.20 (m, 18H), 7.30−7.22 (m, 10H), 7.01 (t, J = 7.5 Hz, 2H), 6.92 (d, J = 8.5 Hz, 3H), 6.83−6.74 (m, 4H). $^{31}P-\{^1H\}$ NMR (202 MHz, d_6-acetone, 298 K): δ −8.62 (d, J_{AgP} = 400 and 347 Hz, 2P). $^{19}F-\{^1H\}$ NMR (470 MHz, d_6-acetone, 298 K): δ −53.7 (s, 3F), −60.3 (s, 3F). Anal. Calcd for $C_{47}H_{33}AgF_6N_2OP_2$: C, 60.99; H, 3.59; N, 3.03. Found: C, 61.21; H, 3.87; N, 2.84.

Selected crystal data of **4**: $C_{51}H_{41}AgF_6N_2O_2P_2$, M = 925.56, orthorhombic, space group $Pbca$, T = 150(2) K, a = 15.8784(7), b = 21.1674(9), c = 23.6769(10) Å, V = 7957.9(6) Å^3, Z = 8, ρ_{calcd} = 1.545 mg/m^3, F(000) = 3744, λ(Mo Kα) = 0.7107 Å, μ = 0.656 mm^{-1}, crystal size = 0.30 × 0.15 × 0.07 mm^3, 9149 independent reflections collected with (R_{int} = 0.0700), GOF = 1.216, final $R_1[I > 2\sigma(I)]$ = 0.0690, wR_2(all data) = 0.1385, and D-map, max./min. = 0.810/−0.862 e/Å^3.

Preparation of Ag(POP)(fiqro) (5). Similar procedures are employed for the reaction of Ag_2O with POP and fiqroH in CH_2Cl_2, giving yellow crystals with yield: 75%.

Spectral data for **5**: MS (FAB, ^{107}Ag): m/z 1082 [M^+ + ^{107}Ag], 646 [M^+ − fiqro]. ^1H NMR (500 MHz, d_6-acetone, 298 K): δ 8.33 (d, J = 8.5 Hz, 1H), 8.04 (d, J = 9.0 Hz, 1H), 7.74 (d, J = 8.0 Hz, 1H), 7.60 (d, J = 8.5 Hz, 4H), 7.34−7.08 (m, 23H), 7.03 (t, J = 7.5 Hz, 2H), 6.98 (d, J = 8.5 Hz, 2H), 6.81−6.76 (m, 3H), 6.74 (t, J = 7.5 Hz, 1H). $^{31}P-\{^1H\}$ NMR (202 MHz, d_6-acetone, 298 K): δ −7.40 (d, J_{AgP} = 393 and 341 Hz, 2P). $^{19}F-\{^1H\}$ NMR (470 MHz, d_6-acetone, 298 K): δ −52.9 (s, 3F), −59.8 (s, 3F). Anal. Calcd for $C_{51}H_{35}AgF_6N_2OP_2$: C, 62.78; H, 3.62; N, 2.87. Found: C, 62.56; H, 3.86; N, 3.26.

Preparation of Au(PPh$_3$)(fpyro) (6). A 25 mL round bottle flask was charged with NaH (7 mg, 0.29 mmol) in 5 mL of THF, and a solution of 3,5-bis(trifluoromethyl)-2-(2′-pyridyl) pyrrole (fpyroH, 51.3 mg, 0.18 mmol) in 10 mL of THF. After stirring at 0 °C for 15 min, the resulting solution was transferred to the solution of $ClAuPPh_3$ (90.7 mg, 0.18 mmol) in 20 mL of THF. This mixture was stirred for 6 h, and the solvent was then evaporated. Colorless crystals were obtained by diffusion of pentanes into THF at RT. Yield: 115 mg, 85%.

Spectral data for **6**: MS (FAB, ^{196}Au): m/z 738 [M^+]. ^1H NMR (500 MHz, CD_2Cl_2, 298 K): δ 8.08 (d, J = 5.0 Hz, 1H), 7.80 (d, J = 8.0 Hz, 1H), 7.70 (t, J = 8.0 Hz, 1H), 7.64−7.52 (m, 10H), 7.52−7.46 (m, 5H), 7.12 (t, J = 6.5 Hz, 1H), 6.92 (s, 1H). $^{31}P-\{^1H\}$ NMR (202 MHz, CD_2Cl_2, 298 K): δ 32.9 (s, 1P). $^{19}F-\{^1H\}$ NMR (470 MHz, CD_2Cl_2, 298 K): δ −54.4 (s, 3F), −59.5 (s, 3F). Anal. Calcd for $C_{29}H_{20}AuF_6N_2P$: C, 47.17; H, 2.73; N, 3.79. Found: C, 47.06; H, 3.11; N, 3.92.

Selected crystal data of **6**: $C_{29}H_{20}AuF_6N_2P$, M = 738.41, triclinic, space group $P\bar{1}$, T = 150(2) K, a = 8.7933(4), b = 10.1944(4), c = 16.6221(7) Å, α = 73.1230(10), β = 75.2700(10), γ = 64.7300(10)°, V = 1274.71(9) Å^3, Z = 2, ρ_{calcd} = 1.924 mg/m^3, F(000) = 712, λ(Mo Kα) = 0.7107 Å, μ = 5.900 mm^{-1}, crystal size = 0.16 × 0.12 × 0.12 mm^3, 5819 independent reflections collected with (R_{int} = 0.0363), GOF = 1.030, final $R_1[I > 2\sigma(I)]$ = 0.0292, wR_2(all data) = 0.0634, and D-map, max./min. = 1.497/−0.689 e/Å^3.

Both Au(PPh$_3$)(fphro) (**7**) and Au(PPh$_3$)(fiqro) (**8**) were prepared in an analogous manner with yields of 87% and 85%, respectively.

Spectral data for **7**: MS (FAB, ^{196}Au): m/z 814 [M^+]. ^1H NMR (500 MHz, CD_2Cl_2, 298 K): δ 7.93 (d, J = 7.0 Hz, 2H), 7.80 (t, J = 7.5 Hz, 1H), 7.68 (d, J = 8.0 Hz, 2H), 7.48 (t, J = 6.0 Hz, 3H), 7.35 (td, J = 7.5 Hz, 2 Hz, 6H), 7.24−7.16 (m, 6H), 7.09 (s, 1H), 6.95−6.92 (m, 3H). $^{31}P-\{^1H\}$ NMR (202 MHz, CD_2Cl_2, 298 K): δ 32.3 (s, 1P). $^{19}F-\{^1H\}$ NMR (470 MHz, CD_2Cl_2, 298 K): δ −53.8 (s, 3F), −59.3 (s, 3F). Anal. Calcd for $C_{35}H_{24}AuF_6N_2P$: C, 51.16; H, 2.97; N, 3.44. Found: C, 51.21; H, 3.03; N, 3.26.

Selected crystal data of **7**: $C_{35}H_{24}AuF_6N_2P$, M = 814.50, triclinic, space group $P\bar{1}$, T = 150(2) K, a = 10.3486(5), b = 11.5288(5), c = 13.3286(6) Å, α = 83.087(1), β = 85.517 (1°, γ = 76.607(1)°, V = 1533.61(12) Å^3, Z = 2, ρ_{calcd} = 1.764 mg/m^3, F(000) = 792, λ(Mo Kα) = 0.7107 Å, μ = 4.913 mm^{-1}, crystal size = 0.40 × 0.32 × 0.25 mm^3, 7022 independent reflections collected with (R_{int} = 0.0282), GOF = 1.025, final $R_1[I > 2\sigma(I)]$ = 0.0220, wR_2(all data) = 0.0494, and D-map, max./min. = 1.202/−0.680 e/Å^3.

Spectral data for **8**: MS (FAB, ^{196}Au): m/z 789 [M^+ + 1]. ^1H NMR (500 MHz, CD_2Cl_2, 298 K): δ 8.18 (d, J_{HH} = 8.0 Hz, 1H), 7.92 (d, J_{HH} = 8.0 Hz, 1H), 7.78 (d, J_{HH} = 8.0 Hz, 1H), 7.54−7.47 (m, 10H), 7.43−7.34 (m, 6H), 7.32 (d, J_{HH} = 8.0 Hz, 1H), 7.12 (t, J_{HH} = 8.0 Hz, 1H), 6.96 (s, 1H). ^{31}P NMR (202 MHz, CD_2Cl_2, 298 K): δ 32.4 (s, 1P). ^{19}F NMR (470 MHz, CD_2Cl_2, 298 K): δ −53.7 (s, 3F), −59.5 (s, 3F). Anal. Calcd for $C_{33}H_{22}AuF_6N_2P$: C, 50.27; H, 2.81; N, 3.55. Found: C, 50.09; H, 3.20; N, 3.78.

Selected crystal data of **8**: $C_{33}H_{22}AuF_6N_2P$, M = 788.46, monoclinic, space group $C2/c$, T = 150(2) K, a = 13.9852(4), b = 10.6777(4), c = 38.8186(14) Å, β = 97.0350(10)°, V = 5753.1(3) Å^3, Z = 8, ρ_{calcd} = 1.821 mg/m^3, F(000) = 3056, λ(Mo Kα) = 0.7107 Å, μ = 5.236 mm^{-1}, crystal size = 0.40 × 0.36 × 0.22 mm^3, 6565 independent reflections collected with (R_{int} = 0.0284), GOF = 1.120, final $R_1[I > 2\sigma(I)]$ = 0.0253, wR_2(all data) = 0.0517, and D-map, max./min. = 0.999/−1.311 e/Å^3.

Photophysical Measurements. Steady-state absorption and emission spectra in both solution and solid were recorded with a Hitachi (U-3310) spectrophotometer and an Edinburgh (FS920) fluorimeter, respectively. Phosphorescence lifetime measurements were performed with an Edinburgh FL 900 photon-counting system. Further details, including the procedures for calculating emission quantum yields, were elaborated in a previous report.[15] As for quantum yield measurements in the solid state, an integrating sphere (Labsphere) was applied, in which the solid sample film was prepared via a vapor deposition method and was excited by a series of Ar^+ laser lines, depending on the sample absorption region. The resulting luminescence was acquired with an intensified charge-coupled device for subsequent quantum yield analyses.[16]

The <300 ps lifetime of the fluorescence bands in dual-emitting complexes was measured with an Edinburgh OB 900-L time-correlated single photon counting system.[17] The excitation pulses were derived from the third or fourth harmonics of the signal output from a traveling-wave optical parametric amplifier of the white-light continuum (TOPAS-C, Spectra Physics) system, seeded by an 1 kHz Ti:sapphire amplifier (Spitfire Pro, Spectra Physics).[18] After convolution, a system response time of ∼50 ps can be confidently achieved. For measuring the relaxation dynamics of <50 ps, we then switched to the femtosecond transient absorption system. Details of UV/vis/NIR transient absorption measurements have been elaborated in our previous report.[19] Briefly, a similar femtosecond Ti:sapphire amplifier was used as the light source (800 nm), which is split (50%) into two beams; one beam is then converted to the designated excitation wavelength, i.e. 400 nm (the pump beam), by coupling it into a second-harmonic generator. The other 800 nm probe beam is then focused on a 1 mm thick sapphire plate to generate a white light continuum (450−1000 nm), which after passing through the sample cell, is coupled into a 100 μm optical fiber connected to a diode array. The effective time resolution of the ultrafast spectrometer is determined to be about 250 fs.

Scheme 1. Structures of Group 11 Transition Metal Complexes: Cu(I) Complexes 1−3, Ag(I) Complexes 4 and 5, and Au(I) Complexes 6−8

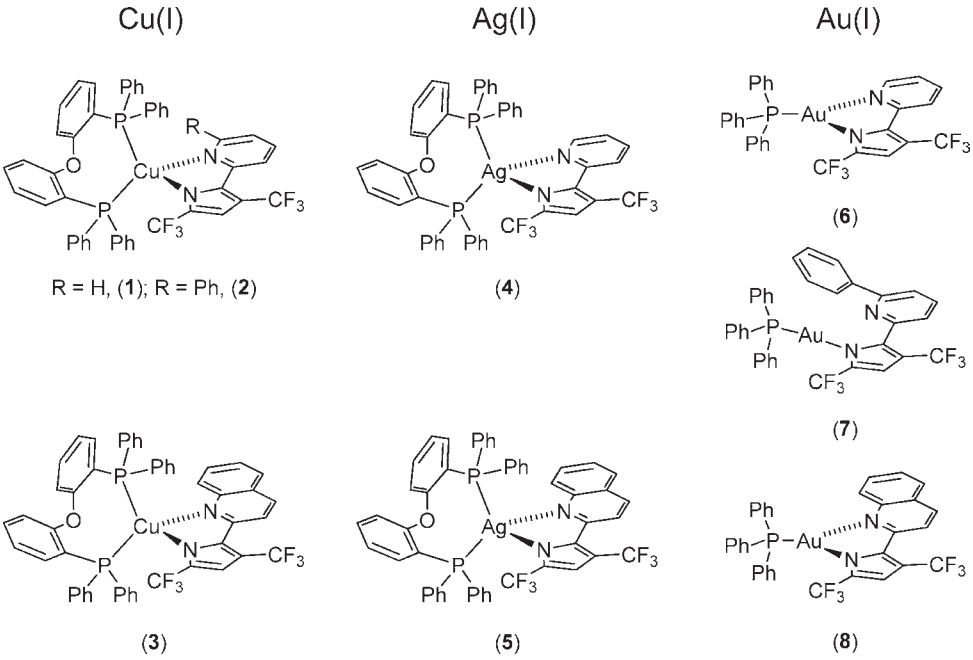

Computational Methodology. Calculations on electronic singlet states of all titled complexes were carried out using the density functional theory (DFT) with B3LYP hybrid functional.[20] A "double-ζ" quality basis set consisting of Hay and Wadt's effective core potentials (LANL2DZ)[21] was employed for the Cu(I), Ag(I), and Au(I) metal ions, and a 6-31G* basis set[22] for the rest of the atoms. The relativistic effective core potential (ECP) replaced the inner core electrons of all metal atoms, leaving only the outer core valence electrons ($ns^2np^6nd^{10}$, $n = 3$, 4, and 5 for Cu(I), Ag(I), and Au(I), respectively) with which to be concerned. Time-dependent DFT (TDDFT) calculations using the B3LYP functional were then performed on the basis of the optimized structures at ground states.[23] Typically, 10 lower triplet and singlet roots of the nonhermitian eigenvalue equations were obtained to determine the vertical excitation energies. Oscillator strengths were then deduced from the dipole transition matrix elements (for singlet states only). All calculations were carried out using Gaussian 03.[24]

Electrochemical Measurement. Cyclic voltammetry (CV) measurements were performed using a BAS 100 B/W electrochemical analyzer. The potentials were recorded using Pt reference electrodes, in anhydrous CH_2Cl_2 with 0.1 M $TBAPF_6$ as the supporting electrolyte, and at the typical scan rate of 100 mV s^{-1}. All data were reported versus NHE and calibrated with ferrocene as the internal standard (0.53 V).

3. RESULTS AND DISCUSSION

3.1. Synthesis and Characterization. Cu(I) metal complexes **1**−**3** were obtained in good yield by mixing an equimolar amount of bis[2-(diphenylphosphino)phenyl] ether (POP) and $[Cu(CH_3CN)_4]BF_4$, followed by addition of 1 equiv of appropriate pyrrole precursors N^NH dissolved in THF solution, where N^NH = fpyroH, fphroH, and fiqroH, for **1**, **2**, and **3**, respectively. On the one hand, these functionalized pyrrole chelates designed according to the supposition that the 2-trifluoromethyl group could increase the steric hindrance around the Cu(I) core and hence inhibit the formation of the flattened conformation at the anticipated MLCT excited state.[25] On the other hand, the selection of POP chelate was also based on its greater rigidity and ability to prevent the solvent attack at the central Cu(I) metal ion by exerting excessive steric protection relative to two monodentate phosphines.[26] These measures are expected to enhance the chemical stability under normal laboratory conditions as well as the emission efficiency (vide infra). Without the ancillary POP chelate, ready aggregation of the copper−pyrrolide fragment occurred, affording a racemic mixture of zwitterionic trimer, such as complexes with formula $[Cu(fpyro)]_3$.[27]

The molecular drawings of Cu(I) metal complexes **1**−**3** are depicted in Scheme 1. Their formulas were first established by mass analysis. Then their spectroscopic characteristics were further confirmed by ^1H, ^{19}F, and ^{31}P NMR, and the purity was verified by subsequent microanalysis. In all cases, the $^{31}P-\{^1H\}$ NMR spectra exhibit a broad peak at around $\delta = -12$, which is independent of the measurement temperature. Apparently, the broadening of the ^{31}P NMR spectrum is caused by the quadruple nuclei ^{63}Cu and ^{65}Cu; both possess a magnetic spin quantum number $I = {}^3/_2$ and have natural abundances of 69% and 31%, respectively.

Crystals of **1** and **2** suitable for X-ray analysis were obtained by slow recrystallization from a CH_2Cl_2/hexane mixture at room temperature. Their ORTEP diagrams are shown in Figure 1, respectively, together with the selected bond lengths and angles. In these two compounds, each of the copper atoms is located in an N_2P_2 distorted tetrahedral environment, in which both the POP and the fphro (or fpyro) moieties are adopting a normal coordination mode. In complex **1**, the Cu−P distances are nearly equal, i.e. Cu−P(1) = 2.2563(9) and Cu−P(2) = 2.2344(9) Å, and it possesses a much widened P−Cu−P bite angle of ∼111°, which is expected for the tetrahedral geometry. Moreover, the molecule possesses two distinctive Cu−N distances, with the Cu−N(pyrrolide) distance of 2.019(3) Å being comparatively shorter than the Cu−N(pyridine) distance of 2.102(3) Å, the

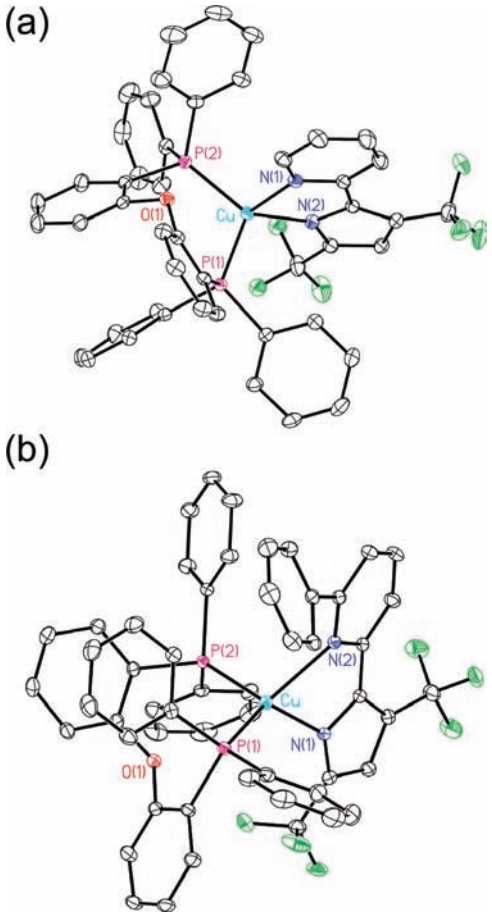

Figure 1. ORTEP diagram of Cu(I) complexes with ellipsoids shown at the 30% probability level. (a) ORTEP diagram of **1** and metric data: Cu−P(1) = 2.2563(9), Cu−P(2) = 2.2344(9), Cu−N(1) = 2.102(3), Cu−N(2) = 2.019(3) Å; N(2)−Cu−N(1) = 80.04(11) and P(2)−Cu−P(1) = 111.95(3)°. (b) ORTEP diagram of **2** and metric data: Cu−P(1) = 2.2500(6), Cu−P(2) = 2.3325(6), Cu−N(1) = 2.0278(17), and Cu−N(2) = 2.2653(17) Å; N(1)−Cu−N(2) = 77.44(7) and P(1)−Cu−P(2) = 111.07(2)°.

result of which reflects the anionic nature of the pyrrolide versus the neutral pyridyl group. In sharp contrast, due to the presence of an *ortho*-substituted phenyl group on the pyridyl fragment of complex **2**, the unfavorable steric repulsion, as demonstrated by the twisted arrangement of the phenyl substituent (see Figure 1b), pushes the adjacent PPh_2 fragment away from the coordinated pyridyl group. The weakening of bonding is clearly shown by the further elongation of the Cu−P(2) and Cu−N(2) distances (c.f. complex **1**) to 2.3325(6) Å and 2.2653(17) Å, respectively, whereas the other Cu−P(1) and Cu−N(pyrrolide) distances are still within the normal range, i.e. 2.2500(6) Å and 2.0278(17) Å, respectively. Notably, the gross conformation of the POP moieties remains unchanged and the respective metric parameters are compatible to those reported in the literature.[26]

In yet another approach, the synthesis of the isoelectronic, second-row Ag(I) analogues was then executed using Ag_2O instead of $[Cu(CH_3CN)_4]BF_4$ in the presence of both POP and respective pyrrolide chelates at RT, giving isolation of two air-stable complexes, Ag(POP)(fpyro) (**4**) and Ag(POP)(fiqro) (**5**), as depicted in Scheme 1. The key spectral features of **4** and **5**, again, involve the ^{31}P NMR splitting pattern of two well resolved

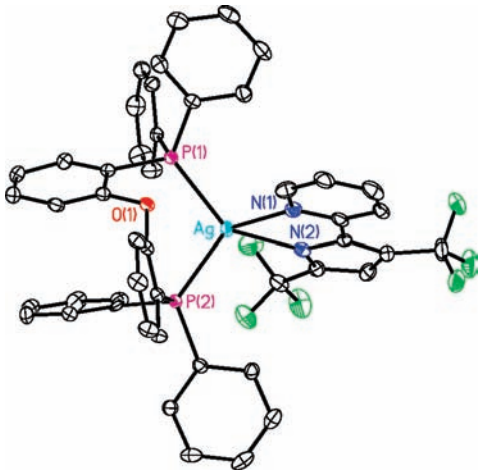

Figure 2. ORTEP diagram of Ag(I) complex **4** with ellipsoids shown at the 30% probability level. Selected bond distances: Ag−P(1) = 2.431(1), Ag−P(2) = 2.473(1), Ag−N(1) = 2.406(4), and Ag−N(2) = 2.265(4) Å. Bond angles: N(1)−Ag−N(2) = 70.79(14) and P(1)−Ag−P(2) = 108.03(4)°.

doublets of nearly equal intensity, a consequence of the direct coupling to both ^{107}Ag and ^{109}Ag nuclei with $I = {}^1/_2$, owing to their natural abundance of 51% and 49%, respectively. This spectral feature also provides the initial spectral confirmation to the formation of Ag(I) metal complexes.

The structure of **4** was then established by X-ray diffraction analysis. As revealed in Figure 2, complex **4** is essentially isostructural to the Cu(I) metal complex **1**, except that all silver−ligand bond distances increase according to the increase of the ionic radius of Ag(I) ion: Ag−P(1) = 2.431(1), Ag−P(2) = 2.473(1), Ag−N(1) = 2.406(4), and Ag−N(2) = 2.265(4) Å. Moreover, the Ag(I) analogue of Cu(POP)(fphro) (**2**) could not be isolated, despite numerous attempts to optimize the conditions. This suggests that the instability very likely originates from the internal steric interaction between the *ortho*-phenyl substituent and its adjacent ancillary POP, which then weakens the coordinative bonding of the anticipated Ag(I) metal complex.

The effectiveness of our endeavors in obtaining all the required d^{10}-metal complexes is further exemplified by the successful preparation of third-row Au(I) metal complexes involving all three pyrrolide chelates, forming Au(PPh_3)(fpyro) (**6**), Au(PPh_3)(fphro) (**7**), and Au(PPh_3)(fiqro) (**8**) depicted in Scheme 1. They were best prepared by first deprotonation of respective pyrrole chelates with NaH in THF, followed by filtration and transferring this solution to a suspension of gold reagent $ClAuPPh_3$ in THF and stirring at RT for an extended period of time (see the Experimental Section for details).

The crystal structures of Au(I) complexes **6**−**8** are then determined, for which the ORTEP diagram and crucial metric parameters are showed in Figure 3 with the metric data enclosed to aid the discussion on the variation of metal−ligand distances and coordination modes. It is notable that all complexes show monomeric structures with no obvious intermolecular Au···Au contacts. In addition, the P−Au−N(pyrrolide) bond angle is found to be essentially linear (163.4−174.1°), which reflects the retention of the typical 2-coordinate metal−ligand arrangement of Au(I) complexes.[28] Meanwhile, the Au−N(pyridyl) distances (2.631−3.004 Å) are elongated versus Au−N(pyrrolide) distances (2.061−2.086 Å). This variation of Au−N distances again

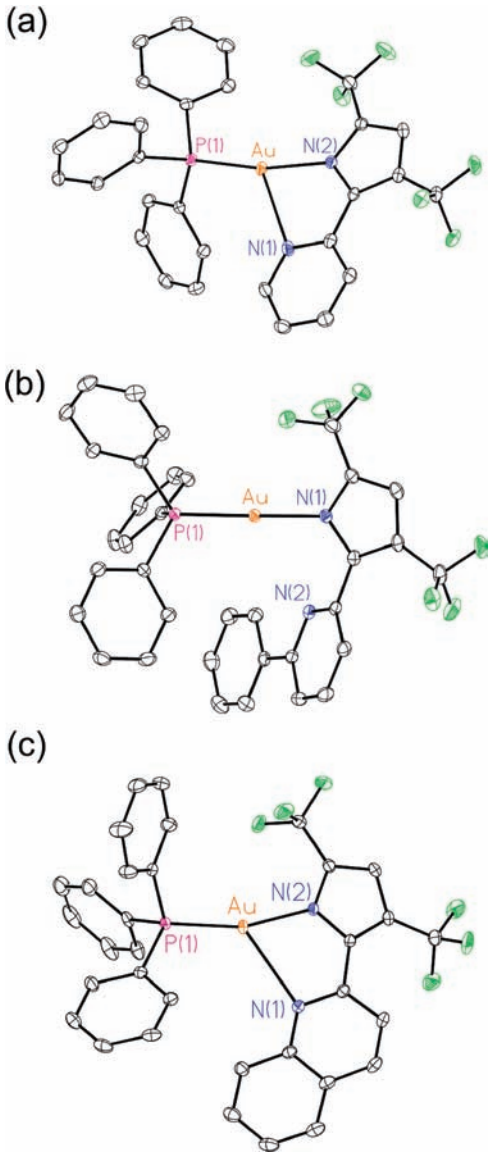

Figure 3. ORTEP diagram of Au(I) complexes with ellipsoids shown at the 30% probability level: (a) ORTEP diagram of **6** and metric data: Au−P(1) = 2.2160(9), Au−N(1) = 2.631(3), and Au−N(2) = 2.082(3) Å; N(1)−Au−N(2) = 69.28(11), P(1)−Au−N(1) = 123.61(7), P(1)−Au−N(2) = 166.91(9)°. (b) ORTEP diagram of **7** and metric data: Au−P(1) = 2.2345(7), Au−N(1) = 2.061(2), Au···N(2) = 3.004(2) Å; P(1)−Au−N(1) = 174.05(6)°. (c) ORTEP diagram of **8** and metric data: Au−P(1) = 2.2207(7), Au−N(1) = 2.681(2), Au−N(2) = 2.086(2) Å; N(1)−Au−N(2) = 69.25(8), P(1)−Au−N(1) = 127.36(6), P(1)−Au−N(2) = 163.38(7)°.

is consistent with the stronger nucleophilicity of the pyrrolide fragment. Furthermore, complex **7** possesses the longest Au−N(pyridyl) distance of 3.004 Å, which is in good agreement with the enhanced intramolecular steric constraint exerted by the *ortho*-phenyl substituent.

3.2. Metal−Ligand−Photophysics Relationship. The room temperature absorption and emission spectra of Cu(I) complexes **1**−**3** are shown in Figure 4. Pertinent photophysical data are listed in Table 1. In CH_2Cl_2, complexes **1** and **2** exhibit multiple absorption peaks in the 200−370 nm region ($\varepsilon > 10^4\ M^{-1}\ cm^{-1}$) that can be attributed to the $\pi\pi^*$ absorption of both N^N and

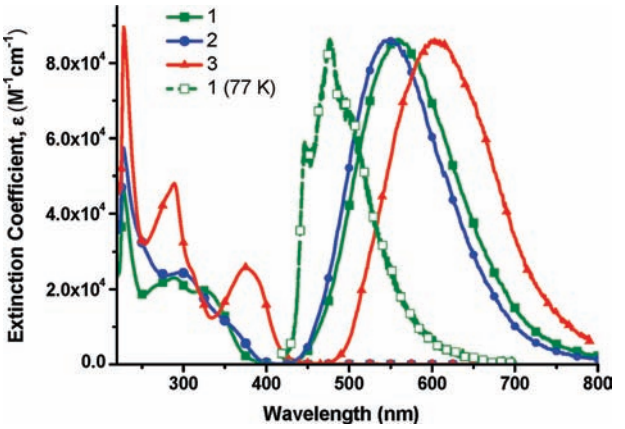

Figure 4. Absorption and normalized emission spectra of Cu(I) complexes **1**, **2**, and **3** recorded in CH_2Cl_2 solution at RT and the emission of **1** in a CH_2Cl_2 matrix at 77 K.

POP ligands. As for complex **3**, the absorption band at 350−400 nm is assigned to the $\pi\pi^*$ transition of the fiqro chelate, which is red-shifted with respect to **1** and **2**, due to the elongation of π-conjugation provided by the quinolinyl fragment. On the other hand, the addition of a phenyl group at the pyridyl site in **2** does not alter the spectral position with respect to that of **1**, indicating that the phenyl ring is not in conjugation with the fpyro moiety, as can be seen from Figure 1. According to the computational results (vide infra), the lowest lying transition for **1**−**3** should contain substantial MLCT (metal-to-ligand charge-transfer) character (Table 2 and Figure 5 for selected frontier orbitals of complex **3**). However, the MLCT band is obscure in the absorption spectra, possibly owing to its small transition probability, i.e. the rather low absorptivity. For instance, in complex **3**, the higher lying transition, e.g. S_2, is essentially localized on the fiqro ligand ($\pi\pi^*$), with oscillator strength f = 0.1628, while the involvement of the Cu(I) metal d-orbital is clearly visualized in S_1, with relatively much lower transition probability (f = 0.0363) and a small difference in energy versus that of the higher lying S_2 state.

In degassed CH_2Cl_2 solution at RT, Cu(I) complexes **1**−**3** all show a single emission band, maximized at 559, 551, and 603 nm (Figure 4) with good quantum yields of 0.34, 0.28, and 0.12, respectively. The emission intensity is drastically quenched by the presence of oxygen in aerated solution. This, together with the calculated radiative decay rate constant of $\sim 10^4\ s^{-1}$ (see Table 1), points out unambiguously that the emission is phosphorescence in origin.

To gain more insight into the emission properties, luminescence spectra of **1**−**3** were also acquired in the 77 K CH_2Cl_2 solid matrix. The resulting emission for complex **1** is shown in Figure 4, while those for **2** and **3** are depicted in Figure S1 of the Supporting Information. For all **1**−**3**, the emission is substantially blue-shifted in the 77 K matrix relative to that recorded at 298 K. Note that the phosphorescence origin of these emission bands remains ascertained due to their >80 μs (instrumental range limited) lifetime. Bearing in mind that the MLCT transition of d^{10} Cu(I) complexes **1**−**3** essentially removes a d electron from Cu(I), thus forming a d^9 Cu(II) metal center, the results can be rationalized by the fact that the original geometry of the tetrahedron-like d^{10} Cu(I) complexes is prone to distortion toward the square-planar-like coordination required by the oxidized d^9 Cu(II) metal center

Table 1. Photophysical and Electrochemical Data of Group 11 Complexes 1−8 Recorded in CH_2Cl_2 at Room Temperature

	λ_{abs} (nm) ($\varepsilon \times 10^{-3}$ M^{-1} cm^{-1})	λ_{em} (nm)[a]	em Q.Y.[a,b]	τ_{obs} (μs)[a]	k_r^P (s^{-1})	E^{ox} (ΔE)[c]	E_{HOMO}[d]
1	228 (47), 289 (23), 325 (20)	559; (481)	0.34; (0.35)	23.9	1.4×10^4	0.43 (81)	0.53
2	228 (57), 296 (24), 357 (10)	551; (490)	0.28; (0.05)	24.8	1.1×10^4	0.54 (67)	0.56
3	228 (89), 289 (48), 375 (26)	603; (553)	0.12; (0.51)	37	3.2×10^3	0.53 (76)	0.61
4	228 (39), 282 (24), 326 (12)	403 [fl], 460, 477, 507; (394 [fl], 446, 476)	0.0075 [fl], 0.0095; (0.14)[b]	176 ps [fl], 138	6.88×10^1	0.74 (irr)	0.65
5	228 (68), 284 (38), 369 (18)	449 [fl], 510, 546, 588; (429 [fl], 495, 532, 573)	0.014 [fl], 0.021; (0.09)[b]	75 ps [fl], 157	1.34×10^2	0.76 (irr)	0.62
6	228 (49), 308 (14)	491; (484)	0.037; (0.40)	124	2.98×10^2	1.04 (irr)	0.79
7	227 (42), 241 (41), 307 (11)	463, 490; (449, 475)	0.01; (0.01)	17.4	5.75×10^2	1.07 (irr)	0.84
8	228 (59), 275 (26), 349 (14)	513, 542, 585; (503, 536)	0.12; (0.04)	79.7	1.46×10^3	1.07 (irr)	0.82

[a] Data recorded in solid state are given in parentheses. Information regarding the fluorescence band is marked with [fl]. [b] The emission quantum yield in solid state is the sum of both fluorescence and phosphorescence bands. [c] E^{ox} represents oxidation potential in V measured in CH_2Cl_2, using 0.1 M $(nBu)_4NPF_6$ as electrolyte and calibrated with ferrocene, and $\Delta E = |E_{pa} - E_{pc}|$ in mV or irreversible peak while marked with "(irr)". [d] The computed energy level of the HOMO in terms of the normal hydrogen electrode (NHE).

in the emissive state, after MLCT excitation.[29] As a result, structural relaxation should take place in the low viscosity solution at 298 K, rendering a bathochromic shift to the emission. On the other hand, such structural distortion is hindered in the 77 K rigid medium so that the phosphorescence emitting states of **1**−**3** retain their ground-state geometries. Similar retardation of structural relaxation is also observed in solid state at 298 K, as evidenced by the >50 nm blue-shift of the phosphorescence peak wavelength relative to that measured in CH_2Cl_2 solution at 298 K (see Table 1 and Figure S2). Thus, the rigidochromism, which has been documented for other transition metal complexes,[29,30] seems to be operative for this class of Cu(I) complexes **1**−**3**.

Supplementary support of the above viewpoint is given by the computational approach. Based on the optimized ground-state tetrahedral geometry, the energy of the lowest lying triplet state is substantially deviated from the phosphorescence peak energy acquired in CH_2Cl_2 at 298 K. For example, the T_1 energy of complex **1** is calculated to be 22,676 cm^{-1} (441 nm in terms of wavelength; see Table 2), which is much higher than the phosphorescence peak energy of 17889 cm^{-1} (559 nm). Similar deviation is resolved for **2** and **3**. However, as shown in Tables 1 and 2, and Figures 4 and S1, the calculated T_1 energies of 441, 435, and 517 nm for **1**, **2**, and **3** are nearly identical with the first vibronic peaks of 446, 453, and 510 nm resolved in the 77 K CH_2Cl_2 matrix, further supporting the proposed rigidochromism for the titled Cu(I) complexes.

More intriguingly, despite the fact that the S_1 state has a substantial MLCT (>20%) contribution, revealed by the frontier orbital analyses (see Table 2 and Figure 5), the T_1 state for **1**−**3** has $\pi\pi^*$ configuration in nature. Spectroscopically, the domination of $\pi\pi^*$ character of the T_1 state is affirmed by the well-resolved vibronic progressions in the 77 K rigid medium. Furthermore, upon careful inspection of the lower-lying electronic excited states for **1**−**3**, it is found that there exists a specific excited state S_m ($m \geq 2$) mainly possessing intraligand $\pi\pi^*$ charge transfer (ILCT) character, which is similar to T_1 (see Table 2).

The above results are of greater value in fundamental photophysics and can be rationalized on the following basis. First of all, due to the good $<\pi|\pi^*>$ overlap integral and thus greater electron exchange energy,[31] the difference in electron repulsion and, hence, the energy splitting between $^1\pi\pi^*$ and $^3\pi\pi^*$ should be greater than that between ^{1}MLCT and ^{3}MLCT. Second, it has been well established that states incorporating significant MLCT character, because of direct involvement of the metal d_π orbital, should invoke significant spin−orbit coupling matrix.[1d,32] Moreover, mixing of MLCT and $\pi\pi^*$ in both singlet (S) and triplet (T) states leads to an S ⟶ T intersystem crossing (ISC) process incorporating the $\langle {}^1d_\pi\pi^*|H_{so}|{}^3\pi\pi^*\rangle$ or $\langle {}^3d_\pi\pi^*|H_{so}|{}^1\pi\pi^*\rangle$ term. The combination of these two factors induces changes of orbital angular momentum, i.e., $d_\pi \rightarrow \pi$ or vice versa, which may effectively couple with the flip of electron spin. As a result, the transition has a significantly large first-order spin−orbit coupling term, which enhances the corresponding singlet−triplet mixing as well as the rate of intersystem crossing.[33] Conversely, for both S and T states possessing pure $\pi\pi^*$ (either intraligand (ILCT) or ligand-to-ligand (LLCT) character), the core metal can be empirically treated as an element that virtually executes a small "external" heavy atom effect as opposed to the "internal" heavy atom effect where a metal d_π orbital is directly involved in MLCT. Together with the lack of changes in orbital angular moment for $S(\pi\pi^*)-T(\pi\pi^*)$ conversion, the $S(\pi\pi^*)-T(\pi\pi^*)$ mixing is small, and hence, a large energy gap between $S(\pi\pi^*)$ and $T(\pi\pi^*)$ states (cf. $S(MLCT/\pi\pi^*)$ and $T(MLCT/\pi\pi^*)$) is expected.

Stemming from the above empirical approaches, for Cu(I) complexes **1**−**3**, due to the substantial MLCT contribution (>20%) in S_1 and, hence, a large spin−orbit coupling matrix, the energy gap between S_1 and its corresponding triplet state is expected to be much reduced. Conversely, an S_m ($\pi\pi^*$) state with negligible MLCT percentage is anticipated to have a larger energy gap with its corresponding triplet state. Thus, despite that the $S_1(MLCT/\pi\pi^*)$ state is ascribed to the lowest excited singlet state for all Cu(I) complexes, its correlated triplet state may not necessarily be the lowest lying triplet state, i.e. T_1. In a more general term, it could be ascribed as the T_n state ($n \geq 2$) shown in Scheme 2. For **1** and **3**, as shown by the calculated data, the T_1 state possesses an essentially pure $\pi\pi^*$ configuration, while the T_2 state is comprised of appreciable MLCT character (see Table 2). We thus conclude that the lowest lying T_1 and second lowest (T_2) triplet states correlate with S_m ($\pi\pi^*$) and S_1 ($MLCT/\pi\pi^*$), respectively. This viewpoint is reaffirmed by a good correlation of the frontier orbitals involved for S_1 and T_2, being mainly contributed by HOMO-1 ⟶ LUMO with substantial MLCT%, as well as for S_m (e.g., $m = 2$ for **3**; see Table 2) and T_1, being mainly associated with the HOMO ⟶ LUMO $\pi\pi^*$ transition. As for **2**, this higher lying T_n is assigned to be T_3 according to the correlation shown in Table 2. This assignment is reasonable, since certain

Table 2. Calculated Energy Levels, Oscillator Strengths (f), and Orbital Transition Analyses for Selected Lower-Lying Transitions of Cu(I) Complexes 1−3

	states	λ_{cal}	f	assignments	MLCT (%)
1	S_1	362.6	0.0021	HOMO-1 → LUMO (60%)	22.73
	S_1	362.6	0.0021	HOMO → LUMO (31%)	22.73
	S_2	359.8	0.0042	HOMO → LUMO (59%)	10.88
	S_2	359.8	0.0042	HOMO-1 → LUMO (29%)	10.88
	S_3	347.5	0.0091	HOMO-1 → LUMO+1 (44%)	14.92
	S_3	347.5	0.0091	HOMO → LUMO+1 (32%)	14.92
	S_3	347.5	0.0091	HOMO → LUMO (5%)	14.92
	S_4	345	0.0812	HOMO → LUMO+1 (85%)	0
	S_4	345	0.0812	HOMO → LUMO (16%)	0
	T_1	441.4 (446)[a]	0	HOMO → LUMO+1 (95%)	0
	T_1	441.4 (446)[a]	0	HOMO → LUMO (10%)	0
	T_2	364.5	0	HOMO-1 → LUMO (26%)	14.33
	T_2	364.5	0	HOMO → LUMO+6 (24%)	14.33
	T_2	364.5	0	HOMO-1 → LUMO+1 (13%)	14.33
2	S_1	356.1	0.006	HOMO-1 → LUMO (74%)	31.12
	S_1	356.1	0.006	HOMO → LUMO (11%)	31.12
	S_1	356.1	0.006	HOMO-1 → LUMO+1 (7%)	31.12
	S_2	353.2	0.0774	HOMO → LUMO+1 (75%)	0
	S_2	353.2	0.0774	HOMO → LUMO (9%)	0
	T_1	434.5 (453)[a],[b]	0	HOMO → LUMO+1 (54%)	0
	T_1	434.5 (453)[a],[b]	0	HOMO → LUMO+3 (35%)	0
	T_1	434.5 (453)[a],[b]	0	HOMO → LUMO+4 (12%)	0
	T_2	391.7	0	HOMO → LUMO+1 (41%)	0
	T_2	391.7	0	HOMO → LUMO+4 (21%)	0
	T_2	391.7	0	HOMO → LUMO+3 (16%)	0
	T_3	365.6	0	HOMO-1 → LUMO (76%)	33.41
	T_3	365.6	0	HOMO-1 → LUMO+3 (6%)	33.41
	T_3	365.6	0	HOMO-1 → LUMO+4 (5%)	33.41
3	S_1	399.9	0.0363	HOMO-1 → LUMO (91%)	36.41
	S_2	388.7	0.1628	HOMO → LUMO (91%)	1.41
	S_2	388.7	0.1628	HOMO-1 → LUMO (5%)	1.41
	T_1	510.3 (517)[a]	0	HOMO → LUMO (86%)	0
	T_1	510.3 (517)[a]	0	HOMO-6 → LUMO (5%)	0
	T_2	430.9	0	HOMO-1 → LUMO (67%)	26.96
	T_2	430.9	0	HOMO-6 → LUMO (17%)	26.96

[a] Values in parentheses denote the first vibronic peaks of the emission spectra measured under 77 K. [b] Value obtained from the halfway point of the slope at the shorter wavelength side.

Scheme 2. Inverted Order of the Lower Lying Singlet-to-Triplet Levels for Cu(I) Complexes 1−3[a]

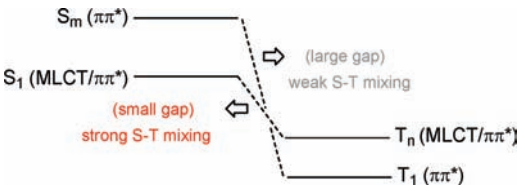

[a] m and n are integer numbers (≥ 2).

higher lying $S_m(\pi\pi^*)$ states may correlate with $T_1(\pi\pi^*)$ due to the presumably large energy gap. Likewise, there is no reason to have $T_1(\pi\pi^*)$ exactly correlated with S_2. For example, as shown in Table 2, good correlation is found between $S_4(\pi\pi^*)$ and $T_1(\pi\pi^*)$ for **1**. It is thus evident that for Cu(I) complexes **1**−**3**, relative to the singlet manifold, the sequence of triplet states has been reversed in the order of energetics shown in Scheme 2. More specifically, according to the data listed in Table 2, the lowest lying S_1(MLCT/$\pi\pi^*$) versus its correlated T_n(MLCT/$\pi\pi^*$) state is delineated to be S_1-T_2, S_1-T_3, and S_1-T_2 for Cu(I) complexes **1**, **2**, and **3**, and their energy gap is calculated to be 0.42, 1.98, and 4.9 kcal/mol, respectively. These values are substantially smaller than the energy gap between $S_m(\pi\pi^*)$ and $T_1(\pi\pi^*)$ for the same series of complexes **1**, **2**, and **3**, which is calculated to be 18.1 (S_4-T_1), 15.3 (S_2-T_1), and 17.4 kcal/mol (S_2-T_1), respectively. Although the current theoretical level and basis sets applied in this study are still subject to uncertainty and, thus, should be treated as a semiquantitative approach, the resulting trend and relationship firmly support the mechanism of large S−T (MLCT/$\pi\pi^*$) versus small S−T ($\pi\pi^*$) mixing proposed above.

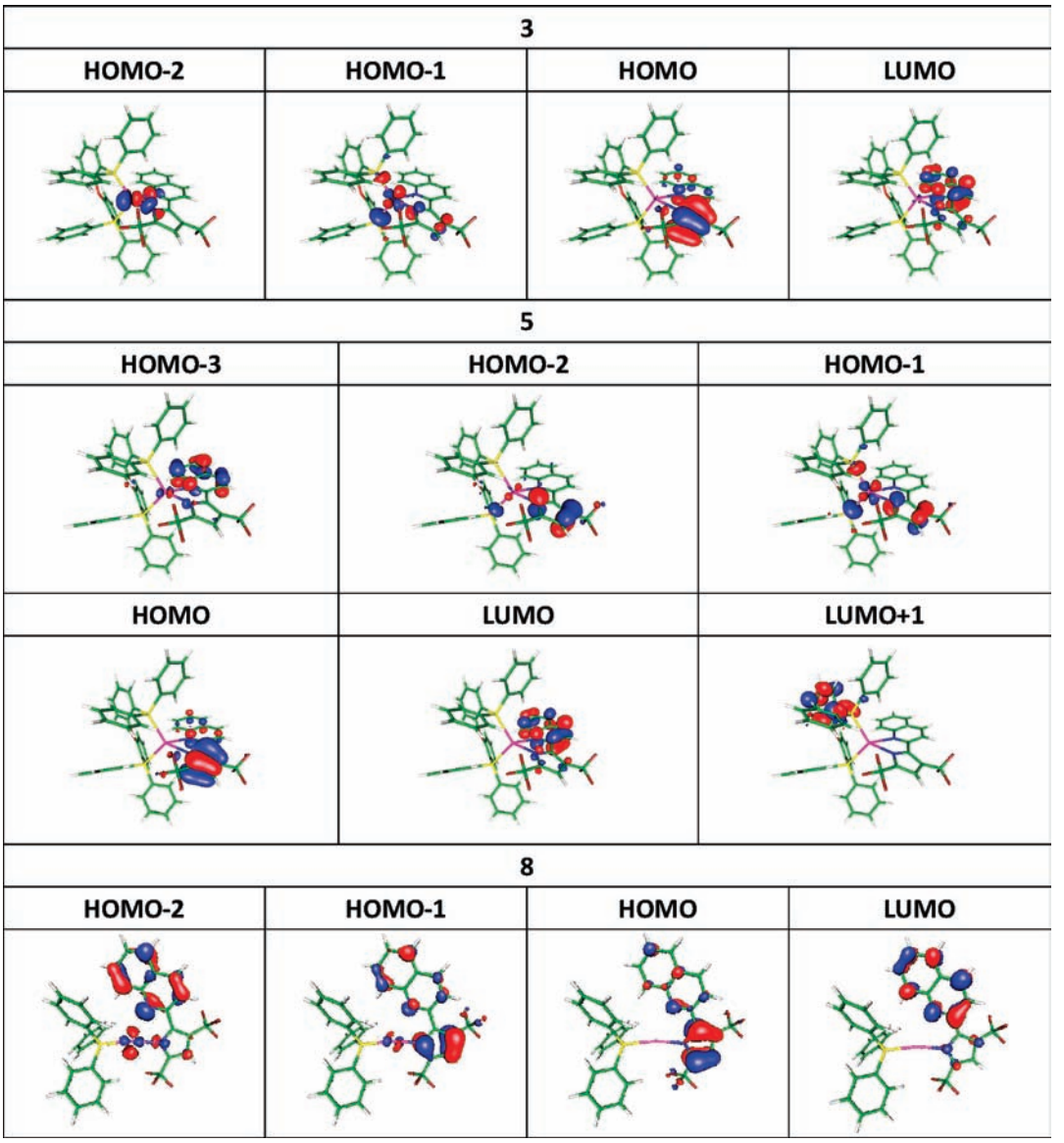

Figure 5. Selected frontier orbitals involved in the lower-lying electronic transitions of group 11 metal complexes **3**, **5**, and **8**.

As the central atom goes down the d^{10} group 11 family from Cu(I) to Ag(I), due to the increase in nuclei charge and, hence, stronger net attracting force, the d orbital should be further lowered in energy, which, in turn, results in an increase of the metal oxidation potential (see section 3.3). As a result, for the lowest lying excited state in both singlet and triplet manifolds, null MLCT contribution is found for Ag(I) complexes **4** and **5** (see Table 3 and Figure 5 for the selected frontier orbitals for **5**), which are isostructural to the Cu(I) complexes **1** and **3**, respectively. For **5**, the first singlet excited state carrying considerable MLCT is S_3 (16%, not shown here), and it is as high as S_6 for complex **4** (14%, not shown). Thus, in brief, for the titled Ag(I) complexes, both S_1 and T_1 are dominated by the ligand-centered $\pi\pi^*$ transition.

As mentioned above, the rate of ISC is strongly influenced by the types of transition involved. More specifically, the corresponding ISC rate constant, k_{isc}, is expressed as

$$k_{isc} \propto \frac{\langle \psi_{T_n} | H_{so} | \psi_{S_1} \rangle^2}{(\Delta E_{S_1 - T_n})^2} \quad (1)$$

where H_{so} is the Hamiltonian for spin−orbit coupling and $\Delta E_{S_1-T_n}$ is the energy difference between S_1 and its correlated T_n states. Though pending quantitative assessment, due to the direct involvement of the metal d_π orbital, the spin−orbit coupling matrix of $|\langle T_n(\mathrm{MLCT}/\pi\pi^*)|H_{so}|S_1(\mathrm{MLCT}/\pi\pi^*)\rangle|$ for Cu(I) complexes **1**−**3** may be greater than that of $|\langle T_1(\pi\pi^*)|H_{so}|S_1(\pi\pi^*)\rangle|$ for Ag(I) complexes **4** and **5**. In other words, since the metal d_π orbitals are not involved in the lowest lying transitions in both singlet and triplet manifolds, the Ag(I) metal center in complexes **4** and **5** simply acts as an external heavy atom, which does not bolster the spin−orbit coupling as effectively as the Cu(I) metal core, defined in this study as an internal heavy atom due to the extensive incorporation of MLCT.

Experimentally, the above viewpoint is fully justified by the steady-state luminescent spectra and relevant photophysical properties. As shown in Figure 6 and Table 1, the Ag(I) complexes **4** and **5** clearly exhibit dual emission, consisting of a fluorescence [λ_{max}: 403 nm (**4**) and 449 nm (**5**)] and a phosphorescence band [λ_{max}: 477 nm (**4**) and 546 nm (**5**)], supporting the slow rate of

Table 3. Calculated Energy Levels, Oscillator Strengths (f), and Orbital Transition Analyses for Selected Lower-Lying Transitions of Ag(I) and Au(I) Complexes 4−8

	states	λ_{cal}[a]	f	assignment	MLCT (%)
4	S_1	364.6	0.0001	HOMO → LUMO (+100%)	0.00
	S_2	340.1	0.0008	HOMO → LUMO+1 (70%)	0.00
	S_2	340.1	0.0008	HOMO → LUMO+2 (27%)	0.00
	T_1	430.0	0	HOMO → LUMO+4 (+91%)	0.00
	T_1	430.0	0	HOMO → LUMO+9 (+10%)	0.00
	T_2	365.3	0	HOMO → LUMO (90%)	0.00
	T_2	365.3	0	HOMO → LUMO+9 (7%)	0.00
5	S_1	385.0	0.1725	HOMO → LUMO (96%)	0.00
	S_2	353.0	0.0026	HOMO → LUMO+1 (99%)	0.00
	T_1	499.9 (492)	0	HOMO → LUMO (83%)	0.00
	T_1	499.9 (492)	0	HOMO-3 → LUMO (6%)	0.00
	T_2	414.2	0	HOMO-3 → LUMO (51%)	2.56
	T_2	414.2	0	HOMO-2 → LUMO (14%)	2.56
	T_2	414.2	0	HOMO → LUMO (11%)	2.56
6	S_1	345.5	0.0093	HOMO → LUMO (97%)	0.00
	S_2	343.6	0.0057	HOMO → LUMO+1 (97%)	0.00
	T_1	426.7	0	HOMO → LUMO+3 (80%)	0.00
	T_1	426.7	0	HOMO → LUMO (9%)	0.00
	T_1	426.7	0	HOMO → LUMO+7 (8%)	0.00
	T_1	426.7	0	HOMO → LUMO+1 (7%)	0.00
	T_2	346.2	0	HOMO → LUMO+1 (49%)	0.00
	T_2	346.2	0	HOMO → LUMO (35%)	0.00
	T_2	346.2	0	HOMO → LUMO+7 (13%)	0.00
7	S_1	350.0	0.005	HOMO → LUMO (100%)	0.00
	T_1	409.8	0	HOMO → LUMO+5 (61%)	0.00
	T_1	409.8	0	HOMO → LUMO+6 (19%)	0.00
	T_1	409.8	0	HOMO → LUMO+3 (12%)	0.00
	T_1	409.8	0	HOMO → LUMO+1 (5%)	0.00
8	S_1	360.4	0.1917	HOMO → LUMO (87%)	0.00
	T_1	482.7 (493)	0	HOMO → LUMO (80%)	0.00
	T_1	482.7 (493)	0	HOMO-2 → LUMO (11%)	0.00
	T_1	482.7 (493)	0	HOMO-1 → LUMO (7%)	0.00

[a] Values in parentheses denote the first vibronic peaks of the phosphorescence bands measured under 77 K.

S_1-T_1 intersystem crossing. Dynamically, as listed in Table 1, the observed fluorescence decay time (τ_{obs}) was resolved to be 176 and 75 ps for complexes **4** and **5**, respectively. By knowing the fluorescence yield (Φ_f; see Table 1), the $S_1 \rightarrow S_0$ fluorescence radiative decay time τ_r ($\tau_r = \tau_{obs}/\Phi_f$) is deduced to be 23.4 and 5.35 ns for **4** and **5**, respectively. Assuming that radiationless deactivation pathways other than ISC are minor, the $(176\ ps)^{-1}$ (**4**) and $(75\ ps)^{-1}$ (**5**) for the fluorescence decay could thus be considered as the rate constant of the S_1-T_1 intersystem crossing process, which is apparently much smaller than that ($\geq 10^{12}\ s^{-1}$) reported for, e.g., typical Ir(III) complexes.[19,34]

As for Cu(I) complexes **1**−**3**, supported by the sole phosphorescence observed in steady-state (see Figure 4), k_{isc} is expected to be faster than that of Ag(I) complexes **4** and **5**. Unfortunately, the intersystem crossing rate cannot be resolved from the fluorescence decay (or rise of the phosphorescence) due to the response limit of ~50 ps (see Experimental Section) for the current time-correlated single photon counting setup. Hence, further resolution of k_{isc} is provided by the femtosecond transient absorption measurement. The lack of suitable excitation wavelength prohibits transient absorption measurements for Cu(I) complexes **1** and **2**. Alternatively, the transient absorption experiment was carried out using **3**. By monitoring the triplet−triplet absorption at 590 nm, as shown in Figure 7, a single exponential rise component of 1.1 ps is resolved. Taking the fast growth of triplet−triplet absorption to be mainly associated with S_1-T_n intersystem crossing, the k_{isc} of $(1.1\ ps)^{-1}$ for **3** is larger than its Ag(I) counterpart **5** by more than 50-fold. It is also noteworthy that the fast $S_1 \rightarrow T_1$ intersystem crossing process of ~10 ps has recently been reported for other Cu(I) complexes.[35] Thus, despite the fact that the Cu(I) core ($Z = 29$) is less of a heavy atom than the Ag(I) counterpart ($Z = 47$), the significantly larger k_{isc} for Cu(I) complexes **1**−**3** (c.f. Ag(I) analogues **4** and **5**) can be rationalized by fast $S_1(MLCT/\pi\pi^*) \rightarrow T_n(MLCT/\pi\pi^*)$ ISC for **1**−**3** versus slow $S_1(\pi\pi^*) \rightarrow T_1(\pi\pi^*)$ for **4** and **5**.

Going further down the periodic table while replacing the central metal atom with the heaviest core, Au(I) complexes **6**−**8** exhibit absorption spectra resembling those of their Ag(I) counterparts **4** and **5** (see Figure 8 and Table 1, and also Figure 5

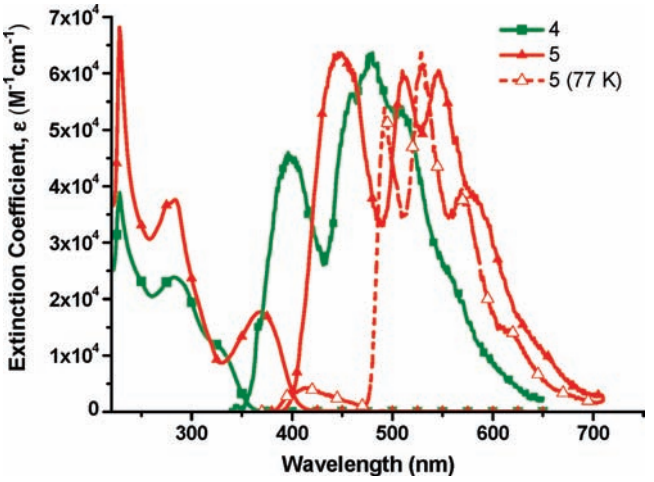

Figure 6. Absorption and normalized emission spectra of Ag(I) complexes **4** and **5** recorded in CH_2Cl_2 solution at RT and the emission of **5** at 77 K.

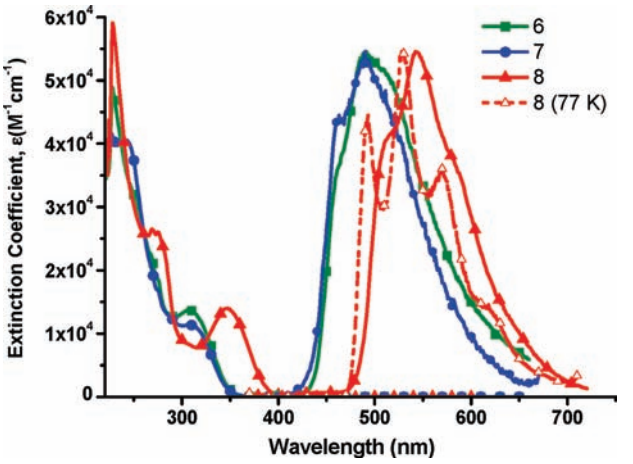

Figure 8. Absorption and normalized emission spectra of Au(I) complexes **6**, **7**, and **8** recorded in CH_2Cl_2 solution at RT and the emission of **8** at 77 K.

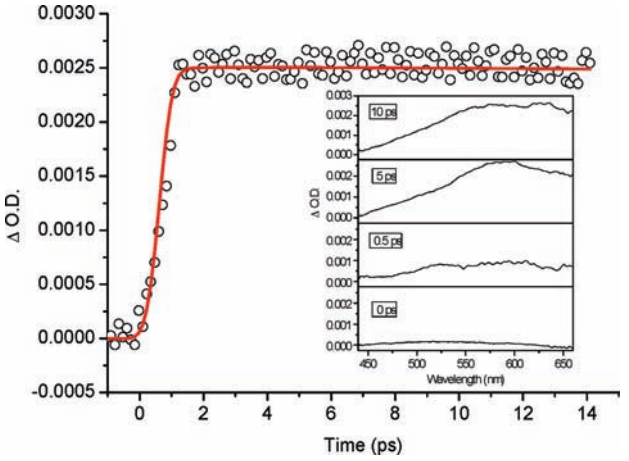

Figure 7. Rise dynamics of triplet−triplet absorption of **3** monitored at 590 nm in CH_2Cl_2. A single exponential rise time is fitted to be 1.1 ps. Inset: The selected transient absorption spectra at various delay times, with excitation wavelength λ_{ex} = 400 nm.

for the selected frontier orbitals of **8**). It has been reported that the metal d orbital of the Au(I) core is even lower in energy compared to those of the Cu(I) and Ag(I) complexes,[36] so that the lowest lying state should be dominated by the ligand-centered $\pi\pi^*$ transition in both singlet and triplet manifolds. This viewpoint is also firmly supported by the computational results listed in Table 3, concluding null MLCT contribution for both S_1 and T_1 states. In sharp contrast to the dual emission (fluorescence/phosphorescence) resolved in **4** and **5**, however, the emission spectrum of Au(I) complexes **6**−**8** consists solely of phosphorescence (see Figure 8). In fact, for **6**−**8**, the large energy separation between S_1 ($\pi\pi^*$) and T_1 ($\pi\pi^*$) states can be perceived via the large Stokes-shift for the phosphorescence emission, defined as the difference in peak wavelength between (the lowest lying) absorption and emission. The large S_1-T_1 ($\pi\pi^*$) energy gap is also evidenced by the calculated values 15.5, 12.3, and 20 kcal/mol for complexes **6**, **7**, and **8**, respectively, according to Table 3.

Scheme 3. Correlation between the Lower Lying Singlet and Triplet Levels for Ag(I) and Au(I) Complexes 4−8[a]

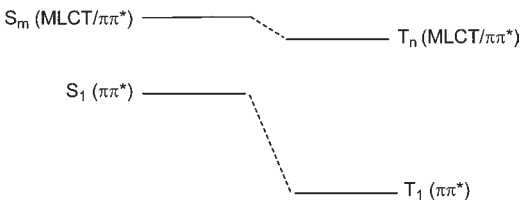

[a] *m* and *n* are integer numbers (≥2).

On the basis of the above discussion, the correlation between the lower lying single and triplet levels for Ag(I) and Au(I) complexes **4**−**8** can be depicted in Scheme 3. Upon excitation, the S_1 state of the Ag(I) and Au(I) complexes, which possesses essentially only the ligand-centered $\pi\pi^*$ character, in theory, should not alter the optimized geometry for the d^{10} configuration. Therefore, unlike the cases of Cu(I) complexes **1**−**3**, structural deformation is not expected to take place for **4**−**8** in the excited state. Experimentally, this viewpoint is firmly supported by the emission spectra acquired in the 77 K rigid medium. As shown in Figures 6 and 8, the emission spectra of Ag(I) complex **5** and Au(I) complex **8**, for example, show similar peak wavelengths and spectral profiles for their phosphorescence bands between 298 and 77 K in CH_2Cl_2, as opposed to the substantial spectral difference observed for the Cu(I) complexes **1**−**3** (vide supra).

Evidently, without MLCT involvement in the lower lying excited states, the Au(I) core also acts as an external heavy atom. Approximating the metal ion as hydrogen-like, a simplified approach predicts that the rate constant of ISC is proportional to Z^8, where Z stands for the atomic number.[37] With the highest atomic number among group 11 elements, the Au(I) core (Z = 79) is expected to induce a stronger external heavy atom effect than that of the Ag(I) core (Z = 47), facilitating the intersystem crossing for complexes **6**−**8** (c.f. Ag(I) complexes **4** and **5**). An attempt to resolve k_{isc} for **6**−**8** via monitoring the lifetime for the fluorescence band (which is not observable in steady state) or the rise time of the phosphorescence by a

dx.doi.org/10.1021/ja2026568 |*J. Am. Chem. Soc.* 2011, 133, 12085–12099

time-correlated single photon counting experiment was not successful due to the much larger k_{isc}, i.e. >$(50\ ps)^{-1}$. We also made efforts in an attempt to resolve k_{isc} via femtosecond transient absorption for complex **8** in CH_2Cl_2 (λ_{ex}: 266 nm). Unfortunately, complex **8** was subject to photodecomposition under such high energy excitation. Nevertheless, the instrumental response-limited time constant (>$(50\ ps)^{-1}$) of k_{isc} for **6**−**8** attests to accelerated intersystem crossing relative to that of Ag(I) complexes **4** and **5**.

As to harvest the $T_1 \rightarrow S_0$ phosphorescence via its radiative transition, the rate constant k_r^p can be expressed as follows:

$$k_r^p \propto \langle \psi_{S_0} | H_{er} | \psi_{T_1} \rangle^2 \approx \gamma \frac{\langle \psi_{S_1} | H_{so} | \psi_{T_1} \rangle^2 \mu_{S_1}^2}{(\Delta E_{S_1 - T_1})^2},$$

$$\gamma = \frac{16\pi^3 10^6 n^3 E_{em}^3}{3h\varepsilon_0} \qquad (2)$$

where H_{er} denotes the electric dipole operator created by the electric magnetic field, μ_{S_1} is the $S_0 \rightarrow S_1$ transition dipole moment, E_{em} represents the T_1-S_0 energy gap in cm^{-1}, and n, h, and ε_0 are the refractive index, Planck's constant, and the permittivity in vacuum, respectively.[30a,38]

As evidenced by the similar absorption extinction coefficients (see Figures 4, 6, and 8 and Tables 1), for simplicity, the $S_0 \rightarrow S_1$ transition dipole moment μ_{S_1} is assumed to be the same for all complexes **1**−**8**. Together with the approximation that E_{em} is the same for all of them, the simplification makes it feasible to correlate $\langle \psi_{S_1} | H_{so} | \psi_{T_1} \rangle^2 / (\Delta E_{S_1-T_1})^2$ with the phosphorescence radiative decay rate constant (k_r). As derived above, $\langle \psi_{S_1} | H_{so} | \psi_{T_1} \rangle^2 / (\Delta E_{S_1-T_1})^2$ increases in the order of Cu(I) complexes (**1** − **3**) > Au(I) complexes (**6**−**8**) > Ag(I) complexes (**4** and **5**), which correlates well with the trend of k_r^p: $10^4\ s^{-1}$ (**1**−**3**) > $3 \times 10^2 \sim 10^3\ s^{-1}$ (**6**−**8**) > $\sim 10^2\ s^{-1}$ (**4** and **5**) (see Tables 1). For both the Ag(I) and Au(I) analogues, negligible MLCT contribution in the emitting T_1 state and, hence, reduction of the T_1-S_1 coupling matrix is manifested by the rather small $T_1 \rightarrow S_0$ radiative (phosphorescence) decay rate constants (k_r^p), on the order of $<10^3\ s^{-1}$. While apparently attributed to the involvement of MLCT, the k_r^p value of $10^4\ s^{-1}$ for the Cu(I) complexes is still less than that of typical Ir(III) complexes ($10^5-10^6\ s^{-1}$) by more than 1 order of magnitude.[19,39] This is mainly due to the much lighter Cu(I) core ($Z = 29$) compared with $Z = 77$ for the Ir(III) core, resulting in a significant decrease of the H_{so} term (see eq 2).

3.3. Electrochemistry. The electrochemical behavior of these group 11 metal complexes was investigated by cyclic voltammetry using ferrocene as the internal standard. The respective redox data are also listed in Table 1. During the anodic scan in CH_2Cl_2, the Cu(I) metal complexes **1**, **2**, and **3** exhibited reversible peak potential at 0.43, 0.54, and 0.53 V, respectively. It is noted that complex **1**, with the smallest degree of π-conjugation at the pyrrolide chelate, shows the lowest potential. This contradictory observation indicates that the oxidation is a localized metal-centered process. In addition, the pyrrolide chelate of **2** and **3** may exert greater steric hindrance on the formation of the square-planar geometry required by the oxidized d^9 Cu(II) metal center. Consequently, their oxidation potentials are expected to be more positive than that of the parent Cu(I) complex **1**; in other words, **1** should give the highest propensity and least amount of barrier in forming the flattened geometry.

Moreover, the oxidation potentials of both Ag(I) and Au(I) complexes were also moved to the more positive region and became irreversible. Such irreversible oxidation versus the reversible nature for Cu(I) complexes (**1**−**3**) indirectly reaffirms the dominant metal participation for Cu(I) complexes as opposed to the pure ligand-centered nature for the Ag(I) and Au(I) counterparts (**4**−**8**), regarding the highest occupied molecular orbitals. This viewpoint is supported by the 0.74 and 0.76 V measured for **4** and **5** in the Ag(I) series and the 1.04, 1.07, and 1.07 V for **6**, **7**, and **8**, respectively, in the Au(I) series. Overall, the oxidation potentials follow the order **6**−**8** > **4**−**5** > **1**−**3**. We also calculated both HOMO and LUMO energies of the titled complexes using the DFT method. As shown in Table 1, the trend of the HOMO energy is also consistent with the above electrochemical measurement (also see Table S1 for the LUMO). Since the metal d orbital should be even lower in energy than the ligand π orbitals for the titled Ag(I) and Au(I) series, the results are consistent with the periodic properties of group 11 metal triads, for which the oxidation potential is in the order Au(I) > Ag(I) > Cu(I). On the other hand, the observed discrepancy between Ag(I) and Au(I) complexes may be alternatively attributed to the difference in coordination environment (four- versus three-coordination).

3.4. OLED Device Fabrication. Following the aforementioned photophysical results and discussion, once the nonradiative decay rate is of a similar magnitude, harvesting phosphorescence depends strongly on the radiative decay rate constant. This seems to be the case for the titled complexes. In degassed CH_2Cl_2 solution, Cu(I) complexes exhibit decent to intense ($\Phi_p = 0.34$) emission, while Au(I) and Ag(I) complexes render weaker and the weakest emission yield, respectively, for which the result correlates well with respect to the order of the radiative decay rate constants (vide supra, see Table 1). Apparently, parts of the nonradiative deactivation pathways are caused by the large amplitude vibration motions that occur in solution, which are expected to reduce or even diminish in solid state, as evidenced by the intense emission for, e.g., Ag(I) complex **4** ($\Phi_p = 0.14$) and Au(I) complex **6** ($\Phi_p = 0.4$) recorded as solid powder. Note that similar dual emissions (fluorescence and phosphorescence) are resolved for the Ag(I) complexes **4** and **5** in solid state, as shown in Figure S3. Nonetheless, for practical concerns such as cost and natural abundance, application to OLEDs is only focused on Cu(I) based phosphors, among which complex **1** is paid special attention due to its high emission quantum yield in both solution and solid state (see Table 1).

In this approach, 1,3-bis(carbazol-9-yl)benzene (mCP) host material and a series of electron transport materials were utilized for fabrication of OLEDs as well as to investigate the carrier balance during device operation. All studied devices consisted of a simplified three-layer architecture of ITO/TAPC (40 nm)/mCP doped with 8 wt % of **1** (30 nm)/electron-transport layer (ETL) (40 nm)/LiF (0.8 nm)/Al (150 nm), for which the graphical configurations and structural drawings of organic materials are depicted in Figure 9. Host material mCP was selected in these studies because it is well-known to allow efficient host-to-guest energy transfer and effective exciton confinement in the emitting layer.[40] After optimization, satisfactory performance was obtained using 1,3,5-tri[(3-pyridyl)phen-3-yl]benzene (TmPyPB) and tris-(2,4,6-trimethyl-3-(pyridin-3-yl)phenyl)borane (3TPyMB) as the electron transport/hole blocking layer for devices A and B, respectively.[41] Device A showed the largest peak brightness of 4988 cd/m^2 at 12.8 V, while peak efficiencies of 2.2%, 6.3 cd/A, 3.7 lm/

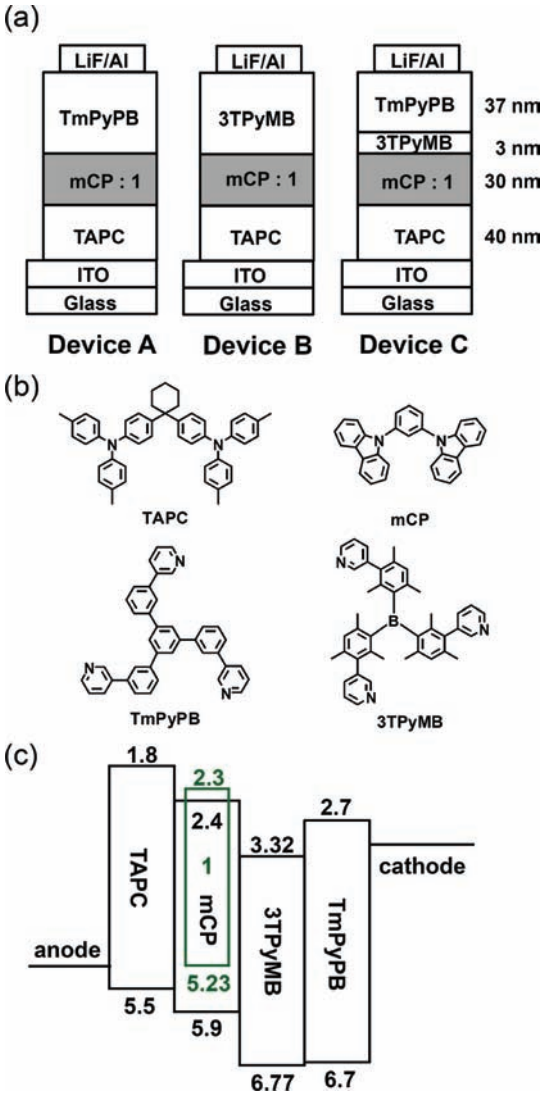

Figure 9. Schematic device structures, and the structural drawing and energy levels of the materials employed for OLED fabrication.

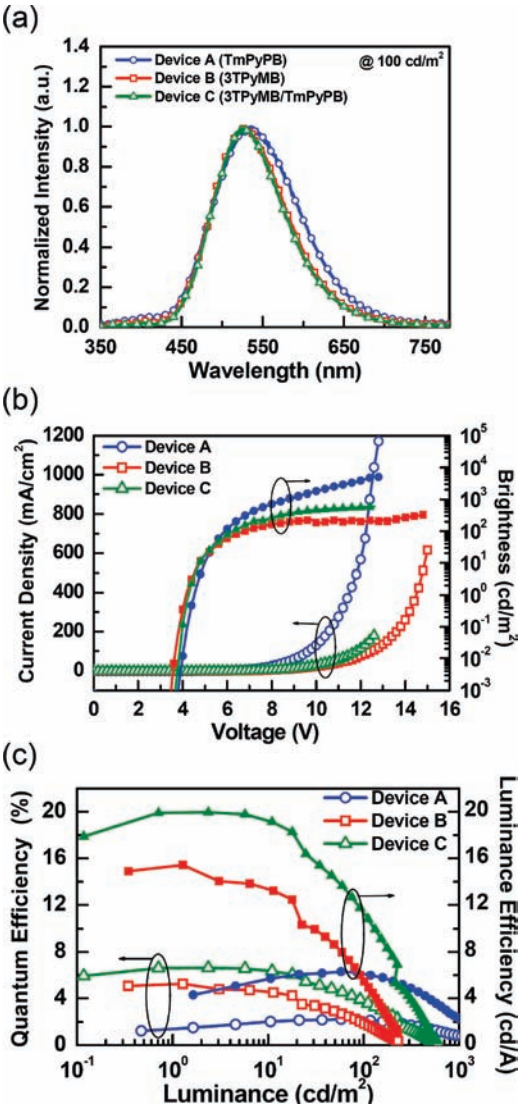

Figure 10. (a) EL spectra, (b) current density−voltage−luminance ($I-V-L$) characteristics, and (c) external quantum efficiency/luminance efficiency vs luminance for the OLED devices A, B, and C fabricated using Cu(I) metal complex **1** as dopant.

W, and 5.3%, 15.4 cd/A, 11.7 lm/W were realized with devices A and B, respectively. The electroluminescence (EL) characteristics and the numeric data are shown in Figure 10 and Table 4. Other tested devices using lower-gap ETLs showed much inferior efficiencies, which are not shown here to save space.

It is noteworthy that both TmPyPB and 3TPyMB possess much larger triplet-energy gap and ionization potential, such that excessive holes are expected to accumulate at the emitting layer (EML)/ETL interface.[41] The accumulation of carriers at the heterojunction causes the build-up of a localized electrical field, which not only alters the carrier transportation but also results in severe exciton quenching.[42] This phenomenon is also related to the difference in the electron transport ability. The electron transport of TmPyPB ($\sim 10^{-3}$ cm^2/(V s)) is faster than that ($\sim 10^{-5}$ cm^2/(V s)) of 3TPyMB by 2 orders of magnitude.[41] The better electron transport capability in TmPyPB might reduce the carrier accumulation at the interface and diminish the localized electrical field. As a consequence, device A exhibited a substantially higher peak luminance of $\sim$5000 cd/m^2. In stark contrast, the peak luminance of device B was merely $\sim$560 cd/m^2, thus confirming the aforementioned quenching effect at higher current densities. In yet another approach, it seems reasonable that one can further reduce the exciton quenching while preserving the carrier balance simultaneously by inserting a thin 3TPyMB layer between the emitting layer and the TmPyPB layer. This thinking led us to fabricate the third OLED, namely device C, which incorporates a double ETL architecture: ITO/TAPC (40 nm)/mCP doped with 8 wt % of **1** (30 nm)/3TPyMB (3 nm)/TmPyPB (37 nm)/LiF (0.8 nm)/Al (150 nm). The total thickness of the ETL was then fixed at 40 nm to make a fair comparison, while 3 nm of 3TPyMB gave the optimal experimental outcome.

As expected, the $I-V-L$ characteristics of device C were similar to those of device B (Figure 10 and Table 4), and the EL efficiencies were higher than those of device B, indicating that the addition of a thin 3TPyMB layer had indeed retarded the electron transport. Although the improvement in peak luminance was only moderate in device C, other device efficiency data have shown

dx.doi.org/10.1021/ja2026568 |J. Am. Chem. Soc. 2011, 133, 12085–12099

Table 4. EL Characteristics of OLEDs with Different ETLs

	η_{ext} (%)		η_l (cd/A)		η_p (lm/W)		V_{on} (V)	max. B (cd/m^2) (V)	CIE coordinates[b]
	[a]	[b]	[a]	[b]	[a]	[b]	[c]		
device A (TmPyPB)	2.2	2.2	6.3	6.1	3.7	3.3	4.5	4988 (12.8 V)	(0.339, 0.500)
device B (3TPyMB)	5.3	1.9	15.4	5.5	11.7	2.6	4.1	558 (15.0 V)	(0.312, 0.515)
device C (3TPyMB/TmPyPB)	6.6	3.8	20.0	11.3	14.9	5.7	4.2	598 (12.6 V)	(0.308, 0.522)
device D (nondoped)	7.8	0.5	23.2	1.4	13.4	0.3	5.2	415 (20.0 V)	(0.322, 0.518)

[a] Maximum efficiencies. [b] Efficiency data recorded at 10^2 cd/m^2. [c] Turn-on voltage measured at 1 cd/m^2.

significant improvement. Overall, device C exhibited peak EL efficiencies of 6.6%, 20.0 cd/A, and 14.9 lm/W for the forward directions. At the practical brightness of 100 cd/m^2, the forward efficiency remained high at around 3.8%, 11.3 cd/A, and 5.7 lm/W. With these encouraging results, these newly developed Cu(I) metal complexes show promising potential in the field of OLEDs.

Nevertheless, according to the energy levels shown in Figure 9c, the HOMO of mCP and the LUMO of 3TPyMB appear well suited to generate exciplex-type emission near 2.6 eV ($\sim$ 480 nm).[43] Electroluminescence from such an interfacial exciplex would overlap with the emission of Cu(I) complex **1** and contribute to the higher efficiency observed. Accordingly, the nondoped device was fabricated to further identify the origin of emission in device C. Thus, a new architecture D was fabricated, which consisted of ITO/TAPC (40 nm)/**1** (30 nm)/3TPyMB (3 nm)/TmPyPB (37 nm)/LiF (0.8 nm)/Al (150 nm). The relevant graphical device diagram and associated efficiency data are shown in Figure S5 of the Supporting Information. As shown in Table 4, the listed data of D were essentially identical to that of all other devices, eliminating the possible formation of exciplex. Moreover, although the peak efficiencies of device D were slightly higher than that of C, the efficiencies dropped notably at higher brightness and the turn-on voltage of D increased to 5.2 V. Such a feature unambiguously confirmed the necessity of the host−guest system used in the present study.

4. CONCLUSION

In conclusion, we have designed and synthesized a series of emissive, group 11 d^{10} transition metal complexes bearing various tailor-made 2-pyridyl pyrrolide chromophores. The compilation of Cu(I), Ag(I), and Au(I) analogues renders systematic discussion on the core-metal dependent variation of the structures feasible. Also, for the first time, the group 11 d^{10} metal core versus its associated photophysical properties is investigated in a comprehensive manner. We have proved unambiguously that, for the titled metal complexes, direct involvement of the d orbital in the lowest lying electronic transition plays a major role in inducing spin−orbit coupling compared to the cases of complexes without metal d orbital involvement in the same transition. The former and latter are dubbed respectively as the internal and external heavy atom effect in this study. As a result, despite the larger atomic numbers for the Ag(I) and Au(I) metal cores, the rate constants of S_1-T_1 intersystem crossing and T_1-S_0 radiative decay of the associated complexes, due to the dominant $\pi\pi^*$ character, are significantly smaller than those of the Cu(I) complexes having appreciable MLCT contribution. Once acting as external heavy atom, our experimental data indicate that the intersystem crossing (ISC) and radiative decay rate constants of group 11 metal complexes increase upon increasing the atomic number down the group. While pending quantitative proof of concept, a similar mechanism is believed to be operative on other transition metal families. Finally, from the application point of view, the low-cost Cu(I) metal element is highly desired for use as lighting materials. As such, complex **1** has been successfully applied as a dopant to fabricate high efficiency OLEDs. In the preliminary approach, the as-prepared device is capable of exhibiting peak EL efficiencies of 6.6%, 20.0 cd/A, and 14.9 lm/W for the forward directions. The combination of fundamental synthetic strategy and encouraging results in potential OLEDs applications should make these group 11 d^{10} metal complexes highly attractive to a broad spectrum of research fields.

■ ASSOCIATED CONTENT

Supporting Information. X-ray crystallographic data file (CIF) and solid state and lower temperature emission spectra of the studied complexes. This material is available free of charge via the Internet at http://pubs.acs.org.

■ AUTHOR INFORMATION

Corresponding Author
ychi@mx.nthu.edu.tw; chop@ntu.edu.tw; chc@saturn.yzu.edu.tw

■ ACKNOWLEDGMENT

This work was supported by the NSC and MEA of Taiwan. We are also grateful to the National Center for High-Performance Computing for computer time and facilities.

■ REFERENCES

(1) (a) Baba, A. I.; Shaw, J. R.; Simon, J. A.; Thummel, R. P.; Schmehl, R. H. *Coord. Chem. Rev.* **1998**, *171*, 43. (b) Armaroli, N. *Chem. Soc. Rev.* **2001**, *30*, 113. (c) Hay, P. J. *J. Phys. Chem. A* **2002**, *106*, 1634. (d) Chou, P.-T.; Chi, Y. *Chem.—Eur. J.* **2007**, *13*, 380. (e) Vlcek, A., Jr. *Top. Organomet. Chem.* **2010**, *29*, 73.

(2) (a) Xiao, L.; Chen, Z.; Qu, B.; Luo, J.; Kong, S.; Gong, Q.; Kido, J. *Adv. Mater.* **2011**, *23*, 926. (b) Sasabe, H.; Kido, J. *Chem. Mater.* **2011**, *23*, 621. (c) Chen, Z.-Q.; Bian, Z.-Q.; Huang, C.-H. *Adv. Mater.* **2010**, *22*, 1534. (d) Zhao, Q.; Li, F.; Huang, C. *Chem. Soc. Rev.* **2010**, *39*, 3007. (e) Wong, W.-Y.; Ho, C.-L. *Coord. Chem. Rev.* **2009**, *253*, 1709. (f) Wong, W.-Y.; Ho, C.-L. *J. Mater. Chem.* **2009**, *19*, 4457. (g) Ulbricht, C.; Beyer, B.; Friebe, C.; Winter, A.; Schubert, U. S. *Adv. Mater.* **2009**, *21*, 4418. (h) You, Y.; Park, S. Y. *Dalton Trans.* **2009**, 1267.

(3) (a) Chou, P.-T.; Chi, Y. *Eur. J. Inorg. Chem.* **2006**, 3319. (b) Chi, Y.; Chou, P.-T. *Chem. Soc. Rev.* **2007**, *36*, 1421. (c) Chi, Y.; Chou, P.-T. *Chem. Soc. Rev.* **2010**, *39*, 638.

(4) (a) Tung, Y.-L.; Lee, S.-W.; Chi, Y.; Chen, L.-S.; Shu, C.-F.; Wu, F.-I.; Carty, A. J.; Chou, P.-T.; Peng, S.-M.; Lee, G.-H. *Adv. Mater.* **2005**, *17*, 1059. (b) Tung, Y.-L.; Lee, S.-W.; Chi, Y.; Tao, Y.-T.; Chien, C.-H.;

Cheng, Y.-M.; Chou, P.-T.; Peng, S.-M.; Liu, C.-S. *J. Mater. Chem.* **2005**, *15*, 460. (c) Fang, C.-H.; Chen, Y.-L.; Yang, C.-H.; Chi, Y.; Yeh, Y.-S.; Li, E. Y.; Cheng, Y.-M.; Hsu, C.-J.; Chou, P.-T.; Chen, C.-T. *Chem.—Eur. J.* **2007**, *13*, 2686.

(5) (a) Vogler, A.; Kunkely, H. *Top. Curr. Chem.* **2001**, *213*, 143. (b) Che, C.-M.; Lai, S.-W. *Coord. Chem. Rev.* **2005**, *249*, 1296. (c) Barbieri, A.; Accorsi, G.; Armaroli, N. *Chem. Commun.* **2008**, 2185. (d) Deaton, J. C.; Switalski, S. C.; Kondakov, D. Y.; Young, R. H.; Pawlik, T. D.; Giesen, D. J.; Harkins, S. B.; Miller, A. J. M.; Mickenberg, S. F.; Peters, J. C. *J. Am. Chem. Soc.* **2010**, *132*, 9499.

(6) (a) Ford, P. C.; Cariati, E.; Bourassa, J. *Chem. Rev.* **1999**, *99*, 3625. (b) Yam, V. W.-W.; Lo, K. K.-W.; Fung, W. K.-M.; Wang, C.-R. *Coord. Chem. Rev.* **1998**, *171*, 17.

(7) (a) Williams, R. M.; De Cola, L.; Hartl, F.; Lagref, J.-J.; Planeix, J.-M.; De Cian, A.; Hosseini, M. W. *Coord. Chem. Rev.* **2002**, *230*, 253. (b) Armaroli, N.; Accorsi, G.; Cardinali, F.; Listorti, A. *Top. Curr. Chem.* **2007**, *280*, 69. (c) Lavie-Cambot, A.; Cantuel, M.; Leydet, Y.; Jonusauskas, G.; Bassani, D. M.; McClenaghan, N. D. *Coord. Chem. Rev.* **2008**, *252*, 2572. (d) Accorsi, G.; Listorti, A.; Yoosaf, K.; Armaroli, N. *Chem. Soc. Rev.* **2009**, *38*, 1690.

(8) (a) Song, D.; Jia, W. L.; Wu, G.; Wang, S. *Dalton Trans.* **2005**, 433. (b) Chou, C.-H.; Yeh, W.-Y.; Lee, G.-H.; Peng, S.-M. *Inorg. Chim. Acta* **2006**, *359*, 4139. (c) Saito, K.; Arai, T.; Takahashi, N.; Tsukuda, T.; Tsubomura, T. *Dalton Trans.* **2006**, 4444. (d) McCormick, T.; Jia, W.-L.; Wang, S. *Inorg. Chem.* **2006**, *45*, 147. (e) Wong, E.; Li, J.; Seward, C.; Wang, S. *Dalton Trans.* **2009**, 1776. (f) Wei, F.; Fang, L.; Huang, Y. *Inorg. Chim. Acta* **2010**, *363*, 2600.

(9) (a) Ma, Y. G.; Che, C.-M.; Chao, H.-Y.; Zhou, X. M.; Chan, W.-H.; Shen, J. C. *Adv. Mater.* **1999**, *11*, 852. (b) Zhang, Q.; Zhou, Q.; Cheng, Y.; Wang, L.; Ma, D.; Jing, X.; Wang, F. *Adv. Mater.* **2004**, *16*, 432. (c) Zhang, L.; Li, B.; Su, Z. *J. Phys. Chem. C* **2009**, *113*, 13968. (d) Min, J.; Zhang, Q.; Sun, W.; Cheng, Y.; Wang, L. *Dalton Trans.* **2011**, *40*, 686.

(10) (a) Armaroli, N.; Accorsi, G.; Holler, M.; Moudam, O.; Nierengarten, J.-F.; Zhou, Z.; Wegh, R. T.; Welter, R. *Adv. Mater.* **2006**, *18*, 1313. (b) Moudam, O.; Kaeser, A.; Delavaux-Nicot, B.; Duhayon, C.; Holler, M.; Accorsi, G.; Armaroli, N.; Seguy, I.; Navarro, J.; Destruel, P.; Nierengarten, J.-F. *Chem. Commun.* **2007**, 3077.

(11) (a) Lotito, K. J.; Peters, J. C. *Chem. Commun.* **2010**, *46*, 3690. (b) Krylova, V. A.; Djurovich, P. I.; Whited, M. T.; Thompson, M. E. *Chem. Commun.* **2010**, *46*, 6696.

(12) Gorin, D. J.; Toste, F. D. *Nature* **2007**, *446*, 395.

(13) (a) Klappa, J. J.; Rich, A. E.; McNeill, K. *Org. Lett.* **2002**, *4*, 435. (b) Ohkura, H.; Berbasov, D. O.; Soloshonok, V. A. *Tetrahedron Lett.* **2003**, *44*, 2417. (c) Chen, J.-L.; Lin, C.-H.; Chen, J.-H.; Chi, Y.; Chiu, Y.-C.; Chou, P.-T.; Lai, C.-H.; Lee, G.-H.; Carty, A. J. *Inorg. Chem.* **2008**, *47*, 5154.

(14) Gubas, G. J. *Inorg. Synth.* **1990**, *28*, 68.

(15) Lin, C.-C.; Chen, C.-L.; Chung, M.-W.; Chen, Y.-J.; Chou, P. T. *J. Phys. Chem. A* **2010**, *114*, 10412.

(16) De Mello, J. C.; Wittmann, H. F.; Friend, R. H. *Adv. Mater.* **1997**, *9*, 230.

(17) Hsieh, C.-C.; Cheng, Y.-M.; Hsu, C.-J.; Chen, K.-Y.; Chou, P.-T. *J. Phys. Chem. A* **2008**, *112*, 8323.

(18) Hsieh, C.-C.; Chou, P.-T.; Shih, C.-W.; Chuang, W.-T.; Chung, M.-W.; Lee, J.; Joo, T. *J. Am. Chem. Soc.* **2011**, *133*, 2932.

(19) Duan, H. S.; Chou, P. T.; Hsu, C. C.; Hung, J. Y.; Chi, Y. *Inorg. Chem.* **2009**, *48*, 6501.

(20) (a) Lee, C.; Yang, W.; Parr, R. G. *Phys. Rev. B* **1988**, *37*, 785. (b) Becke, A. D. *J. Chem. Phys.* **1993**, *98*, 5648.

(21) (a) Hay, P. J.; Wadt, W. R. *J. Chem. Phys.* **1985**, *82*, 270. (b) Wadt, W. R.; Hay, P. J. *J. Chem. Phys.* **1985**, *82*, 284. (c) Hay, P. J.; Wadt, W. R. *J. Chem. Phys.* **1985**, *82*, 299.

(22) Hariharan, P. C.; Pople, J. A. *Mol. Phys.* **1974**, *27*, 209.

(23) (a) Jamorski, C.; Casida, M. E.; Salahub, D. R. *J. Chem. Phys.* **1996**, *104*, 5134. (b) Petersilka, M.; Grossmann, U. J.; Gross, E. K. U. *Phys. Rev. Lett.* **1996**, *76*, 1212. (c) Bauernschmitt, R.; Ahlrichs, R.; Hennrich, F. H.; Kappes, M. M. *J. Am. Chem. Soc.* **1998**, *120*, 5052. (d) Casida, M. E. *J. Chem. Phys.* **1998**, *108*, 4439. (e) Stratmann, R. E.; Scuseria, G. E.; Frisch, J. M. *J. Chem. Phys.* **1998**, *109*, 8218.

(24) *Gaussian 03*, revision C.02; Gaussian, Inc.: Wallingford, CT, 2004.

(25) Tsuboyama, A.; Kuge, K.; Furugori, M.; Okada, S.; Hoshino, M.; Ueno, K. *Inorg. Chem.* **2007**, *46*, 1992.

(26) (a) Cuttell, D. G.; Kuang, S. M.; Fanwick, P. E.; McMillin, D. R.; Walton, R. A. *J. Am. Chem. Soc.* **2002**, *124*, 6. (b) Kuang, S. M.; Cuttell, D. G.; McMillin, D. R.; Fanwick, P. E.; Walton, R. A. *Inorg. Chem.* **2002**, *41*, 3313.

(27) Andino, J. G.; Flores, J. A.; Karty, J. A.; Massa, J. P.; Park, H.; Tsvetkov, N. P.; Wolfe, R. J.; Caulton, K. G. *Inorg. Chem.* **2010**, *49*, 7626.

(28) (a) Yam, V. W.-W.; Chan, C.-L.; Li, C.-K.; Wong, K. M.-C. *Coord. Chem. Rev.* **2001**, *216−217*, 173. (b) Schwerdtfeger, P.; Hermann, H. L.; Schmidbaur, H. *Inorg. Chem.* **2003**, *42*, 1334. (c) De Fremont, P.; Scott, N. M.; Stevens, E. D.; Nolan, S. P. *Organometallics* **2005**, *24*, 2411. (d) Ovejero, P.; Mayoral, M. J.; Cano, M.; Lagunas, M. C. *J. Organomet. Chem.* **2007**, *692*, 1690.

(29) (a) Chen, L. X.; Shaw, G. B.; Novozhilova, I.; Liu, T.; Jennings, G.; Attenkofer, K.; Meyer, G. J.; Coppens, P. *J. Am. Chem. Soc.* **2003**, *125*, 7022. (b) Chen, L. X.; Jenings, G.; Liu, T.; Gosztola, D. J.; Hessler, J. P.; Scaltrito, D. V.; Meyer, G. J. *J. Am. Chem. Soc.* **2002**, *124*, 10861.

(30) (a) Sacksteder, L.; Zipp, A. P.; Brown, E. A.; Streich, J.; Demas, J. N.; DeGraff, B. A. *Inorg. Chem.* **1990**, *29*, 4335. (b) Colombo, M. G.; Hauser, A.; Gudel, H. U. *Top. Curr. Chem.* **1994**, *171*, 143. (c) Weinstein, J. A.; van Slageren, J.; Stufkens, D. J.; Zalis, S.; George, M. W. *J. Chem. Soc., Dalton Trans.* **2001**, 2587.

(31) (a) Turro, N. J. *Modern Molecular Photochemistry*; University Science Books: Mill Valley, CA, 1991. (b) Griffiths, D. J. *Introduction to Quantum Mechanics*, 2nd ed.; Prentice Hall: Upper Saddle River, NJ, 2005.

(32) Cheng, Y.-M.; Li, E. Y.; Lee, G.-H.; Chou, P.-T.; Lin, S.-Y.; Shu, C.-F.; Hwang, K.-C.; Chen, Y.-L.; Song, Y.-H.; Chi, Y. *Inorg. Chem.* **2007**, *46*, 10276.

(33) Chou, P.-T.; Chi, Y.; Chung, M.-W.; Lin, C.-C. *Coord. Chem. Rev.* 2011, DOI: 10.1016/J.CCR.2010.12.013.

(34) (a) Hedley, G. J.; Ruseckas, A.; Samuel, I. D. W. *J. Phys. Chem. A* **2009**, *113*, 2. (b) DeArmond, M. K. *Acc. Chem. Res.* **1974**, *7*, 309.

(35) (a) Iwamura, M.; Takeuchi, S.; Tahara., T. *J. Am. Chem. Soc.* **2007**, *129*, 5248. (b) Leydet, Y.; Bassani, D. M.; Jonusauskas, G.; McClenaghan, N. D. *J. Am. Chem. Soc.* **2007**, *129*, 8688. (c) Iwamura, M.; Watanabe, H.; Ishii, K.; Takeuchi, S.; Tahara, T. *J. Am. Chem. Soc.* **2011**, *133*, 7728.

(36) Nakanishi, W.; Yamanaka, M.; Nakamura, E. *J. Am. Chem. Soc.* **2005**, *127*, 1446.

(37) McGlynn, S. P.; Azumi, T.; Kinoshita, M. *Molecular Spectroscopy of the Triplet State*; Prentice Hall Inc.: Englewood Cliffs, NJ, 1969; Chapter 5, pp 189.

(38) Haneder, S.; Da Como, E.; Feldmann, J.; Lupton, J. M.; Lennartz, C.; Erk, P.; Fuchs, E.; Molt, O.; Münster, I.; Schildknecht, C.; Wagenblast, G. *Adv. Mater.* **2008**, *20*, 3325.

(39) Tsuboyama, A.; Iwawaki, H.; Furugori, M.; Mukaide, T.; Kamatani, J.; Igawa, S.; Moriyama, T.; Miura, S.; Takiguchi, T.; Okada, S.; Hoshino, M.; Ueno, K. *J. Am. Chem. Soc.* **2003**, *125*, 12971.

(40) Holmes, R. J.; Forrest, S. R.; Tung, Y.-J.; Kwong, R. C.; Brown, J. J.; Garon, S.; Thompson, M. E. *Appl. Phys. Lett.* **2003**, *82*, 2422.

(41) (a) Su, S.-J.; Chiba, T.; Takeda, T.; Kido, J. *Adv. Mater.* **2008**, *20*, 2125. (b) Tanaka, D.; Agata, Y.; Takeda, T.; Watanabe, S.; Kido, J. *Jpn. J. Appl. Phys.* **2007**, *46*, L117.

(42) (a) Kalinowski, J.; Stampor, W.; Cocchi, M.; Virgili, D.; Fattori, V. *J. Appl. Phys.* **2006**, *100*, 034318. (b) Reineke, S.; Walzer, K.; Leo, K. *Phys. Rev. B* **2007**, *75*, 125328.

(43) (a) Kolosov, D.; Adamovich, V.; Djurovich, P.; Thompson, M. E.; Adachi, C. *J. Am. Chem. Soc.* **2002**, *124*, 9945. (b) Gebler, D. D.; Wang, Y. Z.; Blatchford, J. W.; Jessen, S. W.; Fu, D.-K.; Swager, T. M.; MacDiarmid, A. G.; Epstein, A. J. *Appl. Phys. Lett.* **1997**, *70*, 1644.